A Review of Inkjet Printing Technology for Personalized–Healthcare Wearable Devices

Journal:	*Journal of Materials Chemistry C*
Manuscript ID	TC-REV-06-2022-002511.R1
Article Type:	Review Article
Date Submitted by the Author:	01-Sep-2022
Complete List of Authors:	Du, Xian; UMass Amherst, Wankhede, Sahil ; UMass Amherst Prasad , Shishir ; Becton Dickinson and Company Morse, Jeffrey; University of Massachusetts Amherst, Institute for Applied Life Sciences Lakal, Narendra; UMass Amherst, Mechanical & Industrial Engineering Shehri, Ali; Massachusetts Institute of Technology

SCHOLARONE™
Manuscripts

A Review of Inkjet Printing Technology for Personalized-Healthcare Wearable Devices

Xian Du*, Sahil P. Wankhede, Shishir Prasad, Ali Shehri, Jeffrey Morse, Narendra Lakal

Xian Du, Sahil P. Wankhede, Narendra Lakal, Department of Mechanical and Industrial Engineering, Center for Personalized Health Monitoring (CPHM), Institute for Applied Life Sciences (IALS), University of Massachusetts Amherst, MA 01003, U.S.A.

E-mail: xiandu@umass.edu

Shishir Prasad, Becton, Dickinson and Company, NJ 07417, U.S.A.

Ali Shehri, Massachusetts Institute of Technology, Cambridge, MA 02139, U.S.A.

Jeffrey Morse, Center for Personalized Health Monitoring (CPHM), Institute for Applied Life Sciences (IALS), University of Massachusetts Amherst, MA 01003, U.S.A.

Keywords: Advanced manufacturing; flexible electronics; personalized healthcare; medical devices; inkjet printing.

Abstract

Personalized healthcare (PHC) is a booming sector in the health science domain wherein researchers from diverse technical backgrounds are focusing on the need for remote patient monitoring. PHC employs wearable electronics, viz. group of sensors integrated on a flexible substrate, embedded in the clothes, or attached to the body via adhesive. PHC wearable flexible electronics (FE) offer numerous advantages including being versatile, comfortable, lightweight, flexible, and body conformable. However, finding the appropriate mass manufacturing technologies for these PHC devices is still a challenge. It needs an understanding of the physics, performance, and applications of printing technologies for PHC wearables, ink preparation, and bio-compatible device fabrication. Moreover, the detailed study of the operating principle, ink, and substrate materials of the printing technologies such as inkjet printing will help identify the opportunities and emerging challenges of applying them in manufacturing of PHC wearable devices. In this article, we attempt to bridge this gap by reviewing the printing technologies in the PHC domain, especially inkjet printing in depth. This article presents a brief review of the state-of-the-art wearable devices made by various printing methods and their applications in PHC. It focuses on the evaluation and application

of these printing technologies for PHC wearable FE devices, along with advancements in ink preparation and bio-compatible device fabrication. The performance of inkjet, screen, gravure, and flexography printing, as well as the inks and substrates, are comparatively analyzed to aid PHC wearable sensor design, research, fabrication, and mass manufacturing. Moreover, it identifies the application of the emerging mass-customizable printing technologies, such as inkjet printing, in the manufacturing of PHC wearable devices, and reviews the printing principles, drop generation mechanisms, ink formulations, ink-substrate interactions, and matching strategies for printing wearable devices on stretchable substrates. Four surface matching strategies are extracted from literature for the guidance of inkjet printing of PHC stretchable electronics. The electro-mechanical performance of the PHC FE devices printed using four surface matching strategies is comparatively evaluated. Further, the article extends its review by describing the scalable integration of PHC devices and finally presents the future directions of research in printing technologies for PHC wearable devices.

1. Introduction

Personalized healthcare (PHC) is one of the primary applications of wearable devices. Initial wearable devices included dedicated electronic sensors and gadgets for remotely monitoring various health parameters. For instance, a wearable device was developed at the Tyndall National Institute in Ireland for doctors to hourly trace biometric readings of their patients and help them reply in case of emergencies [1]. However, this device was inconvenient for continuous wearing because of the cumbersome electronic components and enclosure. These types of bulky devices, hence, were not used for PHC in point-of-care or sports and recreational situations.

Modern developments in material science, electronics, and fabrication methods have propelled the evolution of small and light wearable flexible electronics (FE) for PHC. These FE have electronic components and devices for the sensing elements either assembled within or imprinted on the flexible substrate such that they touch the skin or appropriately interface with the body and can be worn on the human body [2]. The versatility of applications, lightweight, and compact structure of FE [3], along with the ever-expanding consumer goods industry, strongly spurred the growth of the FE market [4] and research and development of novel FE. Most wearable electronic devices have been developed that incorporate sensors for continuous monitoring of human vital signs during in-patient procedures [5–20], human activity [21–25], body fluid analysis [26–33], and medical aid [34–46]. These PHC wearable devices can be

integrated with a body area wireless sensing network for PHC, with radio frequency emitters for communicating with the sensors and the readouts [47], and even energy harvesting/storing transducers for making the PHC devices self-sustained for power [48]. Examples of these applications include wearable and flexible prototypes developed for noninvasive monitoring of glucose levels through various body fluids such as blood, tears, and saliva [30–33]. More recently, stretchable electrodes and interconnects, which enable conformal and intimate skin-device contact for PHC, have been a major focus of many leading research groups and companies in this area.

The fabrication of these devices includes the deposition of functional biocompatible materials on conformal and/or non-curvy surfaces in various designs. Most of these fabrication technologies other than printing technologies have lab scale, long throughput time, and complex and expensive processes. As an additive process, printing has the capability of selectively depositing electronically functional ink materials on large-area non-flat surfaces, at a low cost, in a clean process, with very little or no material wastage. Consequently, many printing methods of FE devices have emerged, such as inkjet [49–54], screen [51,55–60], gravure [51,57,60–62], flexography [51,61,63,64], and lithography printing [65]. In these printing processes, ink material is either transferred from the mold surface to the substrate by physical contacts such as in gravure, screen, or flexography printing or dropped from nozzles or openings to the substrate with no physical contact. The recent innovation of these printing technologies has unlocked the potential for FE devices in broad PHC applications with unprecedented functionalities. In the near future, the ever-changing market will be demanding a short throughput time and low cost for manufacturing new PHC FE products. The development of large-scale fabrication methods [10,66,67], such as printing techniques on a roll-to-roll (R2R) platform is called to reduce the cost of PHC FE products and increase accessibility to the public [49,50,68]. However, selecting the best printing techniques for manufacturing PHC FE products is a challenge, which needs an understanding of the physics, performance, and applications of these printing technologies for PHC wearables, and ink preparation and bio-compatible device fabrication. The comparative performance analysis of the printing techniques (inkjet, screen, gravure, and flexography), as well as the inks and substrates, is needed to aid research in PHC wearable sensor design, fabrication, and mass manufacturing.

Moreover, the detailed study of the operating principle, ink, and substrate materials of the most popular printing technologies such as inkjet printing will help identify the opportunities and emerging challenges of applying the printing technologies in the manufacturing of

specific PHC wearable devices. Inkjet printing is digital, mask-free, and hence capable of depositing ink in customized patterns on a variety of flexible/stretchable substrate materials such as paper, metal, glass, rubber, and polymer. For the guidance of inkjet printing of PHC flexible/stretchable electronics, we need to understand in depth the inkjet printing principles, drop generation mechanisms, ink formulations, ink-substrate interactions, and surface matching strategies for successfully printing functional and biocompatible ink materials on flexible/stretchable substrates.

In this article, we will attempt to bridge the gap between wearable FE for PHC and the corresponding printing techniques by reviewing various printing technologies applicable in the PHC domain, especially inkjet printing in depth. We will first review the research landscape of PHC wearable devices including vitals monitoring and medical aid wearables. Then we will focus on the manufacturing technologies for the FE devices, which are dominated by printing technologies. We will further narrow down the focus on one of the most popular printing technologies, inkjet printing, which has numerous advantages like digital control and the flexibility to print on a variety of flexible and stretchable substrates. We will discuss the inkjet printing mechanism, drop generation mechanism, ink formulation, and ink substrate interaction. Narrowing it down further, we will focus on four surface matching strategies for printing PHC stretchable devices and highlight their pros and cons. We comparatively evaluate the electromechanical performance specifying the change of electrical resistance with stretching rate, the number of stretching/bending cycles, and breakdown strain percentage of the FE, printed using four surface matching strategies, along with the functional material and the substrate. Moreover, we will extend the review to the scalable integration of PHC devices and finally present the future directions of research in printing technologies for PHC wearable devices.

The paper is organized as follows: The article is divided into five sections. Section 2 summarizes the review articles for PHC wearable FE with the fabrication technologies. Section 3 focuses on the printing technologies that have been most successful at fabricating for wearable PHC FE devices, especially inkjet printing along with advancements in ink preparation and bio-compatible device fabrication and emerging challenges for printing stretchable devices. Section 4 describes the scalable integration of PHC devices. Section 5 summarizes the findings of the review and presents the future directions of research for the mass manufacturing of PHC devices.

4

2. Related work

The development of FE devices reached the extent that it has become a large subset of wearable devices. Although nonflexible wearable devices are still there, wearable device research focused on FE devices. Wearable devices research has spanned applications across many domains. The largest domain is healthcare which has vast applications such as monitoring the critical human health condition by measuring motion, vital signs, and activity using various sensors (e.g., electrocardiogram (ECG) for heart monitoring, photoplethysmography (PPG) for blood pressure). As shown in Figure 1 [69], these PHC wearable devices can be integrated with a body area wireless sensing network for PHC, with radio frequency emitters for communicating with the sensors and the readouts, and even energy harvesting/storing transducers for making the PHC devices self-sustained for power [48]. A smartphone will receive and further transfer the sensing data to a central database for remote clinical analysis.
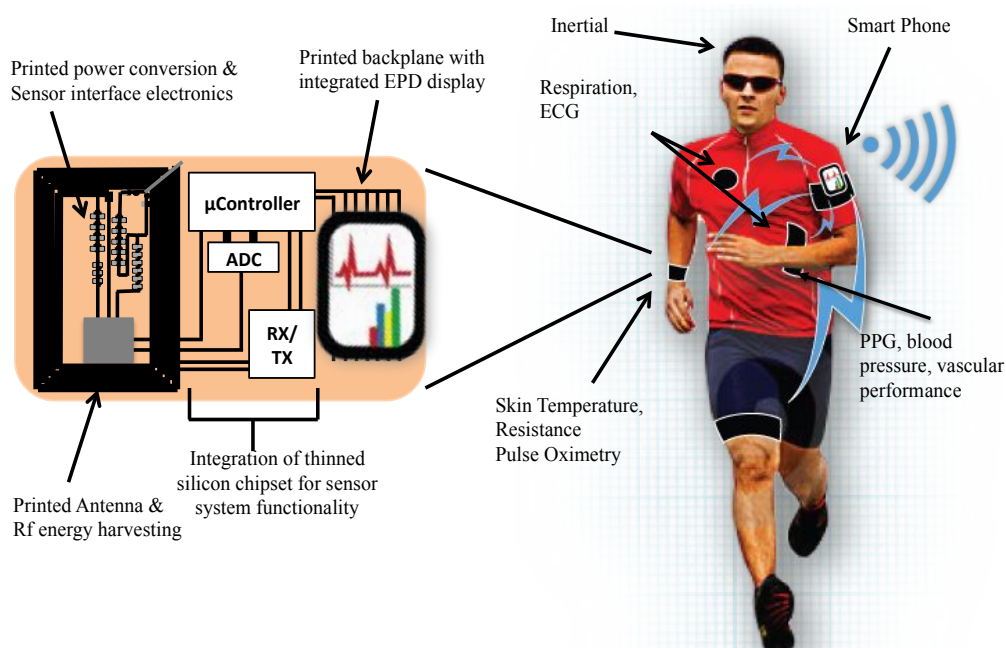

Figure 1. Demonstrator concept of wearable devices and design for PHC Reproduced with permission [69]. Copyright 2016, Jeffry Morse.

2.1. Review of the development of PHC wearable devices

PHC wearable devices have been mostly designed and applied for vitals monitoring and medical aid wearables. Changes in vital signs are crucial, and in many cases are leading indicators of human health. Continuous detection of the vital signs is required both during the in-patient procedures to monitor patient health which aids in taking real-time treatment decisions and in PHM as an early sign of any health complications. In-patient procedures

include monitoring of vital parameters like blood pressure [5–8], body temperature [9–13], ECG monitoring [14,15], pulse oximetry [16–18] as well as monitoring blood flow through the shunts [19,20]. PHM is widely used for human activity monitoring [21–25] and body fluid analysis [26–33]. For example, several prototypes have been developed for the noninvasive monitoring of glucose levels through various body fluids (see Figure 2). Recently, medical aid wearables have emerged to support other medical functions like wound treatment [34,35], drug delivery [36], brain-machine interface [37–40], radiotherapy [41,42], artificial skin [43–45], and ocular disorder treatment [46] with various applications. From the above review, we observe that the major focus of leading research groups and companies in PHC devices is to invent and integrate flexible/stretchable sensors and electrodes and enable skin-intimate or human body-comfortable wearables. These devices are fabricated by depositing functional and biocompatible materials on conformal flexible/stretchable substrates through spin coating, etching, printing, and other technologies. Most of these fabrication technologies other than printing technologies have lab scale, long throughput time, and complex and expensive processes.
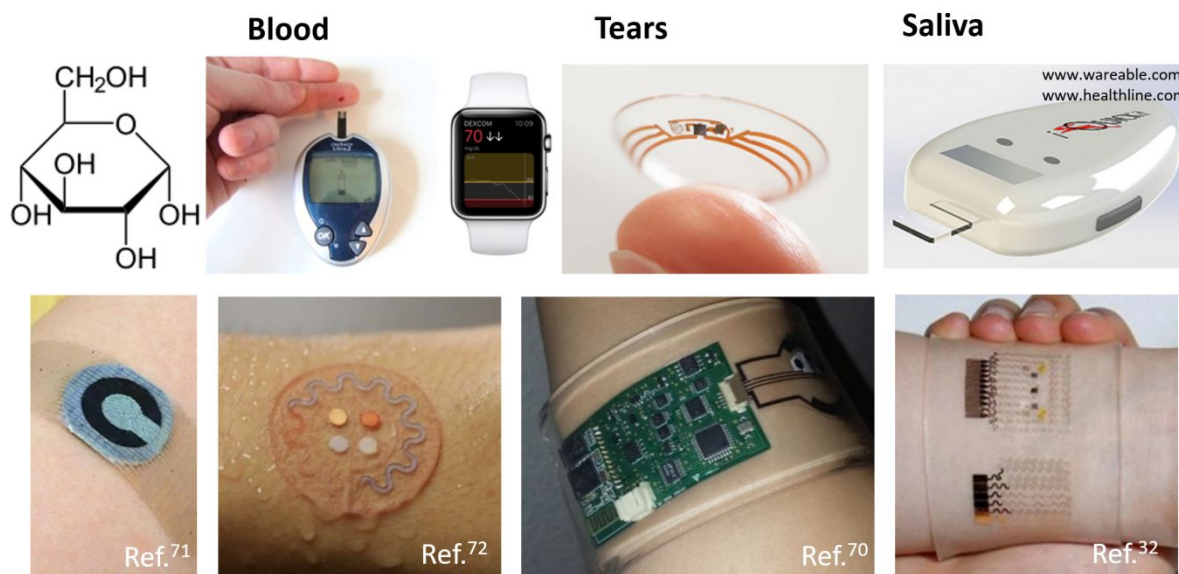

Figure 2. Examples of continuous, noninvasive monitoring of glucose levels through various body fluids. Reproduced with permission [70]. Copyright 2017, National Academy of Science. Reproduced with permission [71]. Copyright 2017, MDPI. Reproduced with permission [72]. Copyright 2016 American Association for the Advancement of Science. Reproduced with permission [32]. Copyright 2016, Springer Nature.

2.2. Review of wearable FE with printing technologies

Many review articles have been published on wearable FE along with the development of printing technologies, which are summarized in Table 1.

Table 1. Summary of the review articles on wearable FE with printing technologies.

Reference	Focus
Li 2015 [73]	Inkjet-printing and biosensor
Khan 2015 [51]	Printing technology for flexible sensors
Gao 2017 [74]	Inkjet printing and wearable devices
Gao 2019 [75]	R2R gravure printing and wearable devices
Khan 2019 [2]	Wearable Sensors
Sreenilayam 2019 [76]	Sensing materials, storage devices, printing technology, and wearable devices.
Zhang 2019 [77]	3D printing and wearable devices
Shrivastava 2022 [78]	Integrated mobile and wearable point-of-care testing
Maddipatla 2020 [79]	Printed flexible sensor
Yan 2020 [80]	Inkjet printing, flexible and wearable devices
Iqbal 2021 [81]	Healthcare wearable devices
Demolder 2021 [82]	Wearable devices

From Table 1 we observe that some review papers are focused on wearable devices with minimal attention to printing techniques such as References [78,81,82]. Few review papers, [2,75–77,79,80] discussed printing techniques and wearable devices with a major focus on ink formulation, flexible/stretchable substrates, and printing strategies. The information mentioned in these review articles is generic and the exact linking of the ink, substrate, and printing techniques for a particular PHC FE device is missing. For wearable devices, the electromechanical performance of the device is of prime importance. These review articles lack the comparison data of electromechanical performance achieved by the wearable devices under bending/stretching loads using the specified conductive ink material, substrate, and printing strategy. Hence, in this review we will focus on the development of printing technology along with advancements in ink preparation and bio-compatible device fabrication.

3. Printing Technologies for PHC Wearable Sensors and Devices

Fabricating wearable devices is challenging since the devices undergo multiple stretching and bending cycles while in contact with the human body. Literature reveals that electronics worn at different locations on the human body are usually subjected to a strain of 15-20% which sets the requirement for strains that wearable FE should be able to withstand [8,9,83].

Recently, printing technologies gained momentum for the manufacturing of FE due to their low cost, high throughput [10,66,67], less material wastage, and facile manufacturing processes [51,84–86]. The printing technologies for wearable FE, in general, can be categorized into two

groups, contact, and non-contact printing techniques. In contact printing, ink is printed by physically touching the surface of the substrate. Gravure printing, offset printing, flexography printing, microcontact printing (μCP), nano-imprinting, and dry transfer printing are typical contact printing techniques. In non-contact printing, the printing ink is discharged through stencil or nozzles onto the substrate and the pattern is printed by the movement of the printhead or the substrate holder in a pre-programmed manner. Screen printing, inkjet printing, and slot-die printing are typical non-contact printing techniques [51]. Non-contact printing techniques have recently gained more popularity because of their advantages in facile operation, versatility for production, good printing resolution, and ease in regulating the printing parameters and control [85–90].

Table 2 demonstrates the printing technologies that have been most successful at fabricating wearable devices for PHC applications to date. These different printing technologies have varying levels of effectiveness for specific applications.

Table 2. Primary printing technologies applied for PHC FE.

	Inkjet Printing	Screen Printing	Gravure Printing	Flexography Printing
Operating Principle	• Deposition of conductive ink droplets through nozzles onto the substrate to form desired pattern/circuit. • Ejection of droplets through thermal, piezoelectric, or electrostatic control.	• Transmission of ink through the stencil. • Control of the pattern through a plate with a screen mesh and a mask.	• Transfer of ink from depressions in a printing plate or roller to a substrate. • Process quality is controlled by a doctor blade, angle and impression pressure, printing speed, and circularity of the gravure cylinder.	• Transfer of ink from a flexible relief plate/roller to the substrate. • Process quality control like Gravure printing.
Adv ant	• Versatile choice of inks/substrates. • Reconfigurable print pattern. • Can print on top of prefabricated flexible	• Well-developed printing technique. • High speed with control over deposition. • High throughput.	• High throughput because of R2R. • High resolution (10s of μm). • Remarkably high precision for	• More versatile material options for substrate and ink than gravure (e.g., carbon nanotube (CNT)).

	circuits. • Less material wastage • Digital controlled ink droplet deposition and location • lower viscosity material can be deposited.	• Easily scalable to a large area. • Low-temperature process, hence reducing the cost. • Easy alignment for the transparent mask. • Low-cost mask/stencil material (e.g. fabrics, steel).	microscale ink thickness.	• R2R compatible. • Better pattern quality in vertical and horizontal directions than gravure printing. • Fragile and stiff substrates can be processed due to flexibility and low pressure imposed on the substrate.
Drawbacks	• Lower throughput. • Energy inefficient. • Nozzle clogging, misfiring. • Limited resolution by droplet size. • Evident budging of lines due to high surface tension in droplets. • The coffee ring effect is caused by the non-uniform distribution of dried solute. • Cluttered droplets at high frequencies.	• Lower resolution patterns than gravure. • Limited by screen mesh (Resolution>30μm). • Speed/throughput comparable to inkjet. • Higher viscosity is required to prevent bleeding and spreading out. • Easy drying of the solvents in ink, resulting in deteriorated print patterns and masks.	• High initial cost and lead time for setting up gravure cylinder. • Inconsistency in maintaining straight printed lines with fine edges. • Pick-out effects due to directions of trenches in printed patterns. • Limited substrate option. • A large degree of control is required for the size and shape of conductive lines. • Challenge to maintain a proper ratio of cell spacing to cell width.	• Complex fabrication of nonporous stamps. • Limitations for large area high-throughput flexo-plate. • ~6-8μm surface roughness of printed pattern. • Peculiar printing defects i.e., Marbling effect. • Complex alignment of multilayers transfer. • Tensile stress is generated during solvent evaporation. • Divergence from designed values is caused by squeezing.

| **Applications** | • Electrodes are used in sensing for analyzing electrochemical reactions.
• On-body tattoo paper passive UHF RFID tags. | • High surface roughness and large wet thickness. | • Graphene high resolution patterned circuit.
• Wearable sweat sensors for detecting molecular composition. | • Gold Nanoparticles (AuNP) based glucose biosensors. |
| **Ref** | 49–54 | 51,55–60 | 51,57,60–62 | 51,61,63,64 |

For selecting a suitable printing technique for wearable FE, it is essential to consider printing specifications like printing speed, minimum line width, line thickness, print resolution, and requirement of the mask for the printing technology [76,79]. Apart from this, substrate, and conductive material to be deposited play a key role. For substrate, it is essential to know the thickness, density, glass transition temperature, melting temperature, coefficient of thermal expansion, Young's modulus, ultimate elongation, bending endurance, surface roughness, and surface energy [91]. The popular substrate materials used for printing wearable FE include Polyethylene terephthalate (PET) [53,60,63,92–96], PolyEthylene naphthalate (PEN) [16,17,41,54,92,97–99], Polyimide (PI) [14,18,19,30,38,41,42,46,55,57,64,100–102], Cellulose paper [35,52,103], PDMS [39,42,93,104–111] and Polyurethane (PU) [112]. The main conductive materials used for fabricating wearable FE include Silver (Ag) [14,21,31,39,46,52–54,60,63,93,94,97,103,107–119], Copper (Cu) [18,25,29,30,41,55,101,120], Gold (Au) [19,28,38,55,64,92,102,106,121,122], Al [102], Pt [37], Graphite [97,105], Poly(3,4-ethylenedioxythiophene) /poly(styrenesulfonate) PEDOT/PSS [14,16,17,53,93,95,98,121], Graphene [21,57,62,123] and CNT [21,60,63,93,99,104]. The conductive material can be deposited in the form of the inks, however, it is essential to know properties like electrical conductivity, surface tension, additives, solvent, and binder used in the ink compatible for each printing techniques [76,79]. Most of the researchers preferred to use silver as conductive material for fabricating their devices. Apart from silver, recently some researchers have started using alternatives such as CNT and copper. In the future, it is expected that a greater variety of materials will be explored and utilized by researchers for fabricating wearable devices.

Table 3 summarizes the printing technologies, substrates, and printing materials reported in the literature, corresponding to various wearable device applications. Applications of wearable devices are classified into two main categories, vitals monitoring, and medical aid wearables. Table 3 indicates that PDMS as substrate, silver as a conductive material, and inkjet printing technology as fabrication process are popular among the researchers.

Table 3. Classification of wearable devices based upon applications, printing technologies, substrates, and ink materials used.

Category	Printing Technologies	Flexible Substrate	Conductive Ink Material	Ref.
Vitals Monitoring : In-Patient Procedure	Tape transfer printing	PI	Indium zinc oxide (IZO)	9
	Screen Printing	PEN	PEDOT: PSS	17
	Aerosol jet printing	Poly (methyl methacrylate) (PMMA) and PI	Ag	46
	Inkjet Printing	Tattoo paper	Ag	52
	Inkjet Printing	PDMS	Ag	108–111
	Inkjet Printing	Kapton	Ag	113
	Inkjet Printing	PET	PEDOT: PSS	95
	Inkjet Printing	PEN	CNT-polymer	99
Vitals Monitoring : PHM	Inkjet Printing	PEN	Ag, Carbon Graphite	97
	Screen Printing	Glucohol tattoo	Ag/AgCl, PB	31
	Screen Printing	PDMS	Graphite	105
	Screen Printing	PET	Graphene, Ag/AgCl	94
	3d printing	Polytetrafluoroethylene (PTFE), PDMS,	AuNP, FeSiCr	106
	Flexography	PI	Au	64
	Inkjet Printing	PEN	PEDOT: PSS	98
	Inkjet Printing	T/C fabric, pure cotton, nylon, and cleanroom wiper	Ag	114
	Inkjet Printing	Teslin paper	Ag	103
	Inkjet Printing	Polyester/cotton fabrics	Ag	124
	Inkjet Printing	Kapton	Ag and ZnO	116
	Inkjet Printing	Kapton	Au	122
Medical Aid Wearable	Inkjet printing	Paper	MnO_2	35
	Screen Printing	Polyethylene (PE), PET, PDMS	Ag, CNT, PEDOT: PSS	93
	Inkjet Printing	Cotton fabrics	Graphene ink	123
	Inkjet Printing	Kapton	Ag	115

Among all printing technologies (see Table 3), inkjet printing is popular for manufacturing wearable devices with high precision and accuracy [107,108]. Many wearable devices were fabricated using inkjet techniques, with their electromechanical performance and applications reported. Table 4 summarizes typical examples of recently fabricated wearable FE devices using inkjet printing technology.

Table 4. Examples of inkjet printing for PHC wearable devices.

Reference	Application	Performance Highlights
Al-Halhouli 2021 [108]	Respiratory Rate (RR) sensors	• Capable to measure at various human postures i.e., sitting at 90°, standing, and lying at 45° with a relative error of 4.49%, 7.29%, and 9.47% respectively.
Wang 2020 [98]	Human body temperature sensor	• Humidity stability from 30% RH to 80% RH. • High-temperature coefficient of resistance (TCR) of -0.77% °C-1 at a sensing range from 25°C to 50°C. • Withstand cyclic bending for 10000 cycles at a bending radius of 5 mm.
Lo 2020 [110]	Arterial pulse pressure sensor	• Sensitivity up to 0.48 kPa-1. • Stretched from 0% to 3% with an increase in resistance of 1200%. • Exhibits, hysteresis-free resistance-strain characteristics.
Ali 2019 [113]	Human body temperature sensor	• Sensitivity of 0.00375°C-1 for the temperature range of 28 °C to 50 °C with a response and recovery times of 4 and 8.5 seconds, respectively. • Bend over diameters in the range of 1 mm to 20mm with negligible change in resistance at 28°C.
Al-Halhouli 2019 [109]	RR sensors	• Withstand axial cyclic strain 2-5% at various stretching speeds of 300,500 and 800 steps/s
Abu-Khalaf 2018 [111]	Heart Rate and arterial oxygen saturation (SpO$_2$)	• Withstand axial strain of 25% with a change in resistance less than 800Ω. • Results were obtained with an average error of ±4.72% for heart rate and ±0.755% for arterial oxygen saturation (SpO2)
Karim 2017 [123]	ECG sensing of the heart	• High-quality heart recordings with an accuracy of 2.1 beats per minute compared to standard heart rate. • Withstand bending test for various chord lengths and 10 home laundry washing cycles.

Shamim 2017 [103]	Antenna for wearable tracking device	• Wi-Fi-based antenna with a communication range of 55m and accuracy of approximately 15 m.
Han 2017 [95]	BTD (body temperature detector) and an HRD (heart rate detector)	• The sensitivity of body temperature detector (BTD) was found to be -31/°C with a linearity of 99.82%. • HR detector had a reliable performance with a standard deviation of 0.85 compared to commercial heart rate sensors and smartwatches.
Krykpayev 2017 [124]	Antenna for wearable tracking device	• Operated at 2.4 GHz for a communication distance of 55 m, with a localization accuracy of up to 8 m. • Withstand bending test up to 90° and for 50 times with resistance change of 30% to 35% with recovery to original values in flat conditions.
Tran 2017 [116]	Photodetector for a wearable UV monitoring	• Response time of 0.3s and high on/off ratio. • No change in performance was observed for bending radii 1mm to 10 mm for 500 cycles.
Khan 2016 [122]	ECG signal and skin temperature	• ECG Electrode provided a 1mVpp ECG signal at 4.7 cm electrode spacing. • The skin temperature sensor was sensitive at normal body temperatures and demonstrated a temperature coefficient, of $\alpha \approx -5.84\%$ K–1. • Withstand bending radii of 10,5 and 2.5 cm for 100 bending cycles with change in room temperature resistance by 0%,0.5%, and 4% respectively.

In the remainder of this section, we focus on several key factors that control the quality of inkjet printing for PHC wearable devices.

3.1. Mechanism of inkjet printing

Inkjet printing is digital, mask-free, and capable of fabricating the complete device in a single and transfer-free process [125]. Inkjet printing can deposit ink in customized patterns on a variety of substrate materials such as paper, metal, glass, rubber, and polymer. The two main mechanisms used in inkjet printing are continuous inkjet (CIJ) and drop-on-demand (DOD). In CIJ mode, an uninterrupted flow of ink drops under the control of the electrostatic field is deposited on the surface of the substrate by a printhead. In DOD inkjet printing, ink droplets are ejected through a nozzle from the reservoir by controlling an acoustic pulse. This pulse can be generated either thermally or piezoelectrically [126]. For fabricating electronic devices, the DOD mechanism is most commonly used [127–129]. In the thermal DOD inkjet printing mode, ink is first heated, which leads to the formation of the vapor bubble. This event in turn forces the ink droplet to eject from the nozzle. In the piezoelectric DOD mechanism, the piezoelectric material is deformed by applying an electric field which in turn squeezes the ink out of the reservoir/cartridge [125,126].

3.1.1. Drop generation in DOD inkjet printer.

Droplet generation in inkjet DOD printers is a complex process. The behavior of liquid drop is mainly characterized by three dimensionless numbers: Reynolds (Re), Weber (We), and Ohnesorge (Oh) numbers [130],

$$\mathrm{Re} = \frac{v\rho a}{\eta} . \qquad \text{1a}$$

$$\mathrm{We} = \frac{v^2\rho a}{\gamma} . \qquad \text{1b}$$

$$\mathrm{Oh} = \frac{\sqrt{W_e}}{Re} . \qquad \text{1c}$$

where ρ, η, and γ are the density, dynamic viscosity, and surface tension of the fluid respectively, v is the velocity, and a is a characteristic length. Apart from the above numbers, Z=1/Oh is considered for denoting stable drop generation. The range of $10 > Z > 1$ is considered stable for drop formation. Higher values of Z lead to the formation of many satellite drops and lower values prevent drop ejection. The effect of the fluid /air surface tension at the nozzle is another factor that acts as a barrier to drop generation. The drop must possess sufficient energy to overcome this barrier. This energy leads to a minimum velocity for drop ejection as recommended by Duineveld et. al. [131].

$$v_{min} = \left(\frac{4\gamma}{\rho d_n}\right)^{1/2}. \qquad\qquad 2$$

where d_n is the diameter of the nozzle. Equation 2. can be written in terms of Weber's number

$$W_e = v_{min}\left(\frac{\rho d_n}{\lambda}\right)^{1/2} > 4. \qquad\qquad 3$$

Lastly, we consider the impact of the ejected drop on the substrate. It is assumed that the drop must impact to leave a single isolated spread drop. Stow and Hadfield [132] established an equation for the onset of splashing.

$$W_e^{1/2}R_e^{1/4} > f(R), \qquad\qquad 4$$

where $f(R)$ is the function of surface roughness only. For a flat, smooth surface $f(R) \sim 50$ [133]. Using equations 2-4 and the limiting values of $Z = 1/Oh$, a plot can be constructed (see Figure 3) to define the printable fluid zone in R_e - W_e region for DOD inkjet printing [130].
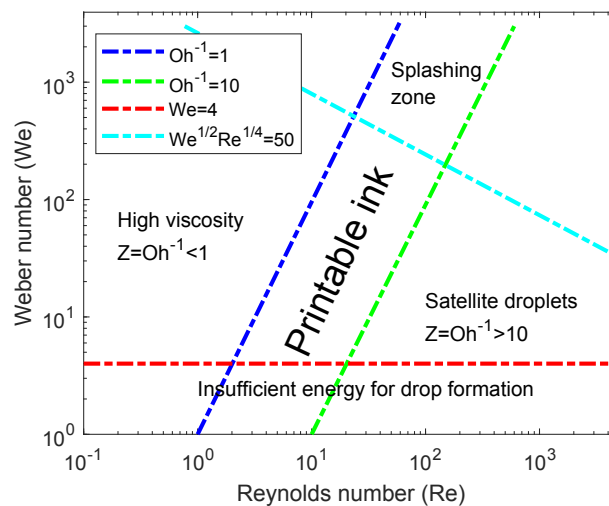

Figure 3. Printable fluid zone.

Drop formation and drop diameter are also influenced by printing parameters like the diameter of the nozzle, waveform, jetting voltage, cartridge temperature, stand-off distance, and humidity. The diameter of the nozzle regulates the size of the drop deposited and thus the resolution of the printing [134]. The volume of the drop can be controlled by waveform parameters; velocity can be controlled by the jetting voltage and cartridge temperature and geometry of the drop can be controlled by jetting voltage and waveform parameters [135]. Stand-off distance i.e., the distance between the nozzle and the substrate influences drop position accuracy, resolution, and formation of the satellite droplets Figure 4 [136]. A stand-off distance of approximately 2-3 mm is maintained in DOD printing [137]. Constant and appropriate relative humidity provides a stable printing process and maintains uniformity in the molecular activities (e.g. polymers and biomolecules) [138].
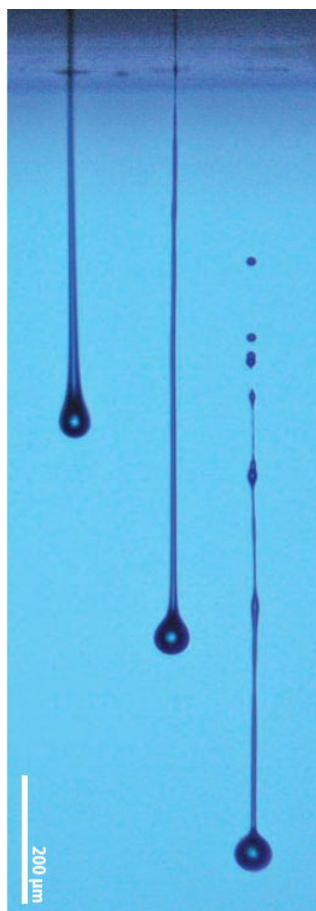
16

Figure 4. Image of three drops ejected from a DOD printer using a high-speed photographic camera illustrating different stages of drop formation. From left to right: the drop forms a single ejected liquid column that rapidly forms a leading droplet followed by an elongated thin liquid tail. The tail breaks up into a trail of satellite droplets behind the leading droplet. Reproduced with permission [136]. Copyright 2008, IOP publishing.

3.1.2. Liquid drop spread on the substrate

After the drop is generated, these drops are ejected from the nozzle and travel directly to the substrate where they spread and undergo a liquid-solid phase change. Physical forces like inertial force, gravitational forces, and capillary forces control the impact of a liquid drop on the substrate [137]. Yarin [139] studied impacting liquid drops for inkjet printing and provided useful findings. They divided the drop impact behavior into several time zones. At the initial stage the impact of the drop is controlled by kinematic behavior i.e., for a duration of approximately t=0.1 or <1 μs, followed by impact-driven spreading and recoil- oscillation. After some time, viscous forces damp the spreading and oscillation and consequently surface tension forces control the behavior. At last, for time t ≈ 10–100 (0.1–1 ms), capillarity force starts dominating and controlling the spreading completely [137,139–141].

In this process, the contact diameter or the footprint d_f is determined by the diameter of the droplet in the air d_a and the equilibrium contact angle θ_{eqm}, defined in the following equation [137,141].

$$d_f = d_a \sqrt[3]{\frac{8}{\tan\frac{\theta_{eqm}}{2}\left(3 + tan^2\frac{\theta_{eqm}}{2}\right)}} \qquad 5$$

From Equation 5, it is evident that the minimum size of the print or the resolution of the inkjet printed pattern depends upon the dimension of the footprint i.e., d_f which is directly proportional to the diameter of the drop in the air i.e., d_a and inversely proportional to the contact angle. Thus, the contact angle which is a function of the surface tension between the air, solid, and liquid governs the size of the pattern to be printed. Normally, the interaction between substrate and ink is governed by 1) modifying the surface tension of the ink by using surfactants 2) changing the surface energy or morphology of the substrate 3) tuning the drying environment 4) developing a substrate with a pre-pattern structure [137,141].

3.1.3. Droplet Coalescence on the substrate

In the Inkjet printing process, two neighboring drops merge to form a liquid bead due to significant contact line pinning. Duineveld [142] examined the behavior of the liquid drops inkjet-printed on a variety of the substrate having different contact angles and formulated an equation below for maximum stable liquid bead width obtained through inkjet printing,

$$w = \sqrt{\frac{2\,\pi\,d_a^3}{3\mathrm{p}\left(\frac{\theta^*}{sin^2\theta^*} - \frac{cos\theta^*}{sin\theta^*}\right)}} \cdot \qquad 6$$

Here w= width of the bead, p is the drop spacing and θ^* is static advancing contact angle not equilibrium contact.

Uniform printing of the patterns is assured by the coalescence of the droplets on the substrate in a straight line without bulging or waving [143]. The process of droplet coalescence is illustrated in Figure 5. It shows the side view and the bottom view of the two consequently printed evaporating colloidal drops, particle deposition processes, and carrier liquid evaporation. From Figure 5, one can observe that the contact line of the 1st drop is pinned, particles move towards the contact line and some particles are deposited at the contact line before the impact of the 2nd drop. After the impact of the 2nd drop, both merge into the 1st drop due to inertia. After merging the drops, the air-water interface oscillates which creates variation in contact angle, relaxation velocity, and local mean radius of curvature of the air-water interface. This oscillation drives the liquid back and forth and brings the particles together. Once the water-air interface achieves equilibrium it forms a circular shape, particles

start flowing towards the edge of the combined drop and the liquid starts evaporating. Finally, particles deposit at the edge of the combined drop [144]. This process can be summarized in three steps 1) Quick merging of the drops 2) rearrangement of the merged liquid droplets 3) deposition and mixing of the particles inside the liquid [143].
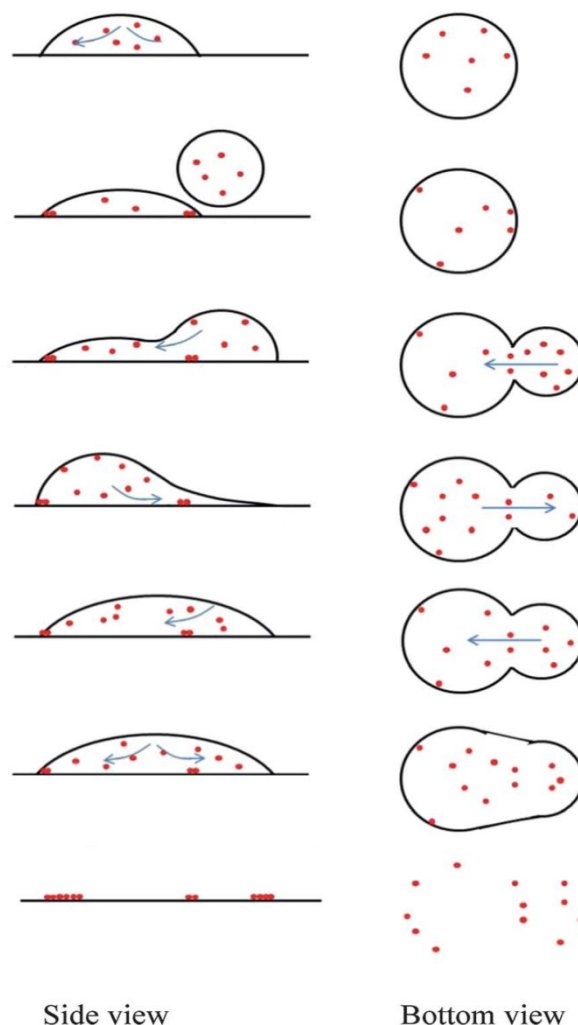

Side view   Bottom view

Figure 5. Schematic of drop impact, coalescence, carrier liquid evaporation, and particle deposition of two consecutively printed evaporating colloidal drops from the side view (left)and bottom view(right). Reproduced with permission [144]. Copyright 2012, Royal society of chemistry.

Further deposition morphology relies heavily upon drop spacing and the delay time. Soltman and Subramanian [145] demonstrated a study explaining the variation of the inkjet-printed line morphologies with the drop spacing. For large values of drop spacing i.e., greater than the drop footprint there is no overlap of the drop which results in the formation of a series of discrete droplets (Figure 6a). For the distance slightly lesser than the drop footprint, coalescence of the drop is observed, resulting in the formation of the "scalloped" liquid beads with no smooth parallel sides. (Figure 6b). Reducing drop spacing further results in the formation of smooth parallel sides (Figure 6c). Finally, if the drop spacing is too small it

results in the formation of bulging unstable lines (Figure 6d). Apart from the drop spacing, delay time between the two adjacent drops is critical since it prevents the droplet coalescence into one large drop and keeps them isolated [143].
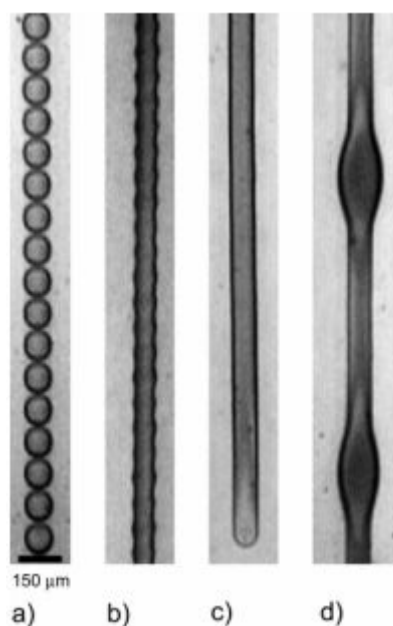

Figure 6. Variation of inkjet-printed morphologies with drop spacing a) Too large drop spacing for drop coalescence forming a series of discrete droplets b) Beginning of coalescence forming scalloped liquid bead (c) Smooth parallel-sided liquid bead d) bulging instability for too small drop spacing. Reproduced with permission [145]. Copyright 2008, American Chemical Society.

3.1.4. Drop solidification on the substrate

Conversion of the liquid drop deposited on the substrate into a solid material is the last step in the printing process. Solidification of the drop is caused by solvent evaporation, however, the increase in solvent evaporation rate causes the drying of the nanoparticles at the edges forming thick layers at the contact line. This phenomenon is known as the coffee stain effect [137,146–148]. Furthermore, Deegan et. al. [146] observed that solvent evaporation near the edge of the drop is faster as compared to the center of the drop because of the large dry substrate surrounding it, which provides rapid vapor transport at the contact line. To compensate for fluid lost due to evaporation more solution will move to the edge of the drop, resulting in the amount of solute transfer towards the contact lines [137,149]. This coffee stain effect [150] plays a vital role in controlling the shape of inkjet-printed drops and leads to the formation of a dual ridged line profile after solidification of the liquid beads depicted in Figure 7.
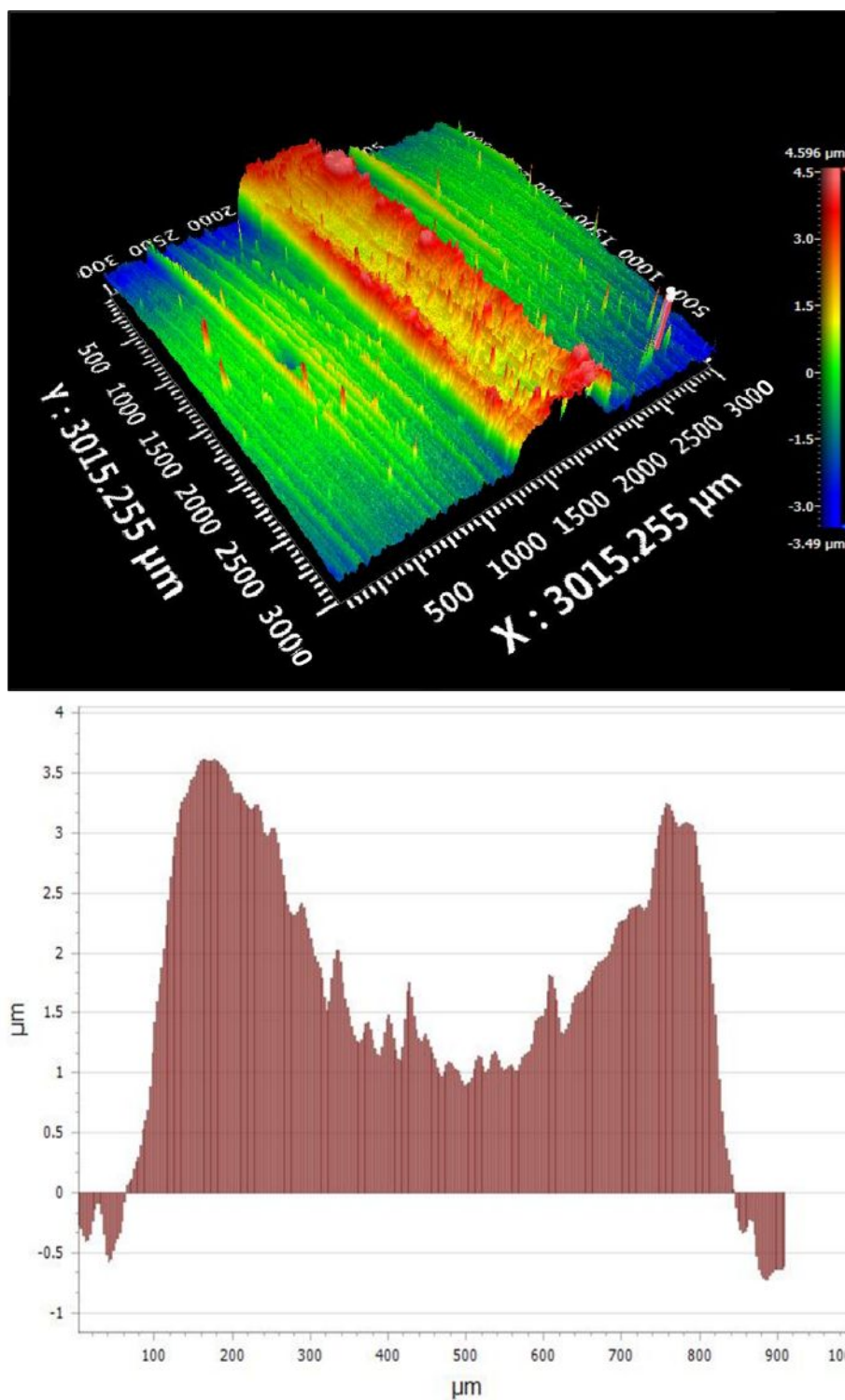
Figure 7. Coffee staining effect for printed silver nanoparticle ink. (a) Interferometric image depicting distinct ridges at the edges of the track formed after drying of the liquid bead. (b) Changes in height across the track are shown by two-line profiles.

Many methods have been proposed to overcome the "coffee ring effect" like increasing the inward Marangoni flow, weakening the outward flow, and preventing droplet pinning [141,151,152]. Marangoni flow is the flow induced by temperature differences and surface tension gradient due to solvent concentration that causes ink particles to flow back to the center of the

21

drop from the edge [146,153]. Hu et.al. developed a co-solvent binder-free black phosphorus (BP) ink with 10 vol% alcohol in N-methyl pyrrolidone (NMP) which prohibited the coffee ring staining effect using the Marangoni flow. It was used for inkjet printing for optoelectronics and photonics, particularly for large-scale printing of quantum dot light-emitting diodes [154]. Liu et. al. inhibited the outward capillary flow by in situ crystallization of perovskite-nanocomposite microarrays with additive polyvinylpyrrolidone (PVP). This aided in controlling the microarray's morphology [155]. Lately, Al-Milaji et. al. developed a novel "dual-droplet" inkjet printing in which droplets containing colloidal particles were deposited on a supporting droplet. This technique aided the nanoparticles to spread and self-assemble in a densely packed monolayer at the air-liquid interface which suppressed the coffee-ring effect [156]. He et. al. demonstrated an ice drying method for inhibiting the coffee ring effect on multiple substrates. The inkjet-printed various patterns with uniform deposition by controlling the ice-drying temperature and time delay. This process induced a temperature gradient Marangoni flow which suppressed the coffee-ring effect [157]. One more way to reduce the coffee ring effect is to use a complex solvent containing fluids with different vapor pressure. Enhanced vapor pressure rate will decrease the difference in evaporation rate and thus reduce the coffee staining [145].

In addition to the inkjet printing mechanism, the quality of the printed pattern depends on the ink formulation and surface energy matching between the ink and the substrate [125].

3.2. Ink formulation

Viscosity and surface tension of the ink is the most important property to be considered while inkjet printing. The viscosity of the ink for inkjet printing should be below 20mPas. If the viscosity of the ink is high, no droplet will be ejected. The lower the viscosity, the greater the velocity and quantity of ink ejected through the nozzle. Surface tension plays a crucial role in maintaining the spherical shape of the drop after coming out of the nozzle. A typical range of surface tension suitable for inkjet printing is from 28mN/m (e.g. Xylene) to 350mN/m (for molten solder) [126]. In addition to surface tension and viscosity, the post-processing treatment is sintering - which involves the merging of the particles - plays a key role in determining the conductivity of the printed electronic circuit of the wearable device.

The conductivity of printed patterns for the ink with silver (Ag) nanoparticles (AgNP) highly depends on the sintering time and temperature. With the increase in sintering temperature or time, the AgNP with larger size begins to melt and contact with each other to form a conductive path. The small AgNPs pack into the gap between the large ones. Finally, the

AgNPs sinter together to create a 3D conductive network [125,158]. Additionally, conductivity can be improved by using AgNPs with broad size distribution [158].

Table 5 shows the list of commercial inks and their properties like surface tension, viscosity, resistivity, and sintering temperature. Note, to avoid clogging of nozzle it is recommended the particles in the ink should be 1/100th the size of the nozzle [159].

Table 5. List of commercial inks and their properties (adapted from [160]).

Ink Functional Material	Vendor	Commercial Name	Solvent	Particle Size	Resistivity	Viscosity (mPa.s)	Surface Tension (mNm)	Sintering Temperature (°C)
Silver	Advanced Nano Products	DGP-40LT-15C	Triethylene glycol monoethyl ether (TGME)	50 nm	11 μΩ-cm	10-17	35-38	120-150
	Colloidal Ink, Co	Drycure Ag-J	Glycerol	15-20 nm	5 μΩ-cm	8-12	30	120
	Harima Electronic Materials	NPS-J	-	12 nm	-	9	-	120
	Harima Electronic Materials	NPS-JL	-	7nm	-	11	-	220
	InkTec	TEC-IJ-010	-	-	-	9-15	30-32	100-150
	InkTec	TEC-IJ-060	-	-	-	5-15	27-32	100-150
	Sigma Aldrich	Ag NP	Terpineol	-	-	10-13	28-31	150-300
	Novacentrix	Metalon JS-B25HV	Ethylene glycol	60 nm	2.8 μΩ-cm	8	30-32	125
	Novacentrix	Metalon JS-B40G	Diethylene glycol monobutyl ether	60-80 μm	2.6 μΩ-cm	8-12	28-32	180
	Novacentrix	JS-A102	2,2'-Oxybisethanol	40-60 nm	2.8 μΩ-cm	8-12	25-30	140

	Novacentrix	JS-A211	Diethylene glycol	30-50 nm	7.7-73 μΩ-cm	8-12	28-32	120
Nickel	Applied Nanotech	Ni-IJ70	-	0.070 μm	20 μΩ-cm	16-25	26-31	Photosintered
Copper	Novacentrix	ICI-002HV	-	110-130 nm	7.5-10.8 μΩ-cm	9-12	28-32	Pulseforge
	Applied Nanotech	Cu-IJ70	-	0.060 μm	5-7 μΩ-cm	10-20	20-30	Photosintered
Gold	Harima Electronic Materials	NPG-J	-	7 nm	12 μΩ-cm	7	-	250
	Colloidal Ink, Co	Drycure Au-J Solid	Glycerol	-	7.5 μΩ-cm	10	30	120
Polymer	PEDOT AGFA	Orgacon IJ-1005	-	-	-	7-12	31-34	130
Graphene	Sigma Aldrich	Graphene nanoparticle	Ethyl cellulose in cyclohexanone and terpineol	-	-	1	30	250
CNTs	Brewer Science	CNTs	-	-	-	<10	-	110-150

3.2.1. Ink Composition

For ink formulation, it is essential to know the constituent elements of the ink. Inkjet printing inks mainly consist of functional material (solid metal precursors), polymeric resin, additives, and solvents [161]. We will briefly discuss the composition of silver ink.

Functional Material

Silver, Gold, Copper, and Nickel are widely used functional materials. Metal precursors are soluble or dispersible in the solvent medium. They are incorporated into the ink as per their application like electroactivity or conductivity. Silver is considered one of the best options for application as a conductive ink and adhesive, compared to other electrically conductive fillers. This is mainly due to its high thermal and electrical conductivity, chemical stability, and excellent capability of silver oxide to conduct electricity [162,163].

Polymeric Resin

Polymeric Resin is included in the silver ink as a stabilizer to prevent agglomeration of the AgNPs. It serves as a capping agent to protect the metal particles against oxidation. Further, it plays the role of a binder to facilitate adhesion between the silver ink pattern and the substrate. Some commonly used polymeric resin examples are Polyvinylpyrrolidone (PVP) which serves as a dispersant and capping agent, and Nitrocellulose which is cheap, durable, and strong adhesive to a wide variety of substrates.

Solvent

A solvent is the carrier of functional material. The viscosity and rheological characteristics of the ink can be determined by the proportion of the solvent in it. The solvent can prevent the blocking of the nozzle during printing and evaporate after the ink deposition on the substrate [163]. Ethylene glycol, toluene, or cyclohexane, methyl-ethyl-ketone (MEK), formic acid, ethyl alcohol, PVP, sodium borohydride, and water are popular solvents used.

Additives

Additives are used to alter the rheological properties of the ink and determine the ink printability and quality of final patterns. The amount of additives in silver ink is < 5% by weight of the overall ink composition. The rheology, wettability, substrate adhesion, dielectric constant, and antifoaming properties of the ink are regulated by the additives. Additives are incorporated into silver ink to regulate the surface tension, particularly for water-based ink due to the high surface tension of water ($\sim 72 \times 10^{-3}$ N/m) compared to substrates ($< 32 \times 10^{-3}$ N/m). Thus, it is essential to control the surface tension of the ink and

ensure that it is lower than the surface energy of the substrate to obtain good printability and adhesion [161].

3.2.2. Bio-compatible inks

Most of the inks discussed in Table 5 are metal-based inks. These inks are used often because of their high electrical conductivity. However, these inks are costly, not environmentally friendly, not biocompatible, and require high sintering temperatures which limit the use of heat-sensitive materials. Thus, researchers are finding alternatives for low-cost, environmentally friendly, biocompatible, and low-sintering temperature inks. In a study, Karim et. al. formulated water-based reduced graphene oxide (rGO) for the e-textile manufacturing process. These inks can be dried at a low temperature of 100°C which prevents damaging heat-sensitive fabrics. Further, it has a viscosity of 1.35mPa s and surface tension of 65mN/m with a sheet resistance of $2.14 \times 10^3 \Omega sq^{-1}$ [164]. Similarly, Yang et.al. developed an environment-friendly conductive graphene/ Thermoplastic Polyurethane (TPU) ink dissolved in green solvent dihydrolevoglucosenone (Cyrene) for fabricating wearable strain sensor for monitoring human joint motion and muscle movement. Adjusting the ratio between the graphene and TPU, the strain sensor exhibited excellent sensitivity and good durability over 5000 cycles [165]. McManus et. al. formulated biocompatible, water-based, ink-jet printable two-dimensional crystal inks using graphene as a functional material, triton x-100 as a solvent, and propylene glycol as co-solvent. The ink has a surface tension of ~40mN/m and viscosity of ~1.37 mPa-s. The ink was used to fabricate smart identification tags for food, drinks, consumer goods, and pharmaceuticals, where inexpensive, lightweight, and easy to assemble components are required [166]. Furthermore, Liang et. al. formulated biocompatible and highly stable conductive ink using natural silk sericin-carbon nanotubes (SSCNT). The SSCNT exhibit high electrical conductivity 42.1±1.8 S/cm and colloidal stability for months. It was compatible with various fabrication techniques like inkjet printing, direct writing, stencil printing, and dyeing. Further, it showed excellent adaptability for various flexible substrates such as papers, PET films, and textiles. The ink was to fabricate ECG sensors, breathe sensors, and electrochemical sensors demonstrating excellent performance in monitoring human health [167]. Farizhandi et. al. developed a bio-ink using composite polymer consisting of poly(glycerol-co-sebacate) acrylate (PGSA) as non-conducting polymer and zinc as conducting metal. It exhibited excellent conductivity, biocompatibility, biodegradability, printability, and mechanical properties of elastomers. Further, it was used for fabricating implantable and flexible electronic devices using the 3D

printing technique [168]. Li et. al. formulated a biocompatible aqueous ink by encapsulating liquid metal nanodroplets of gallium and indium (EGaIn) into microgels of marine polysaccharides. This ink could maintain chemical and colloidal stability for a period of >7d and demonstrated the electrical conductivity of 4.8×10^5 Sm^{-1} (siemens per meter) through mechanical sintering. Ink can be used on various substrates by inkjet printing and drop casting techniques. Further, it was used for fabricating wearable sensors, electric-thermal actuators, electronic tattoos, artificial limbs, electric skin, etc [169].

Organic conductive polymers like poly (3,4-ethylenedioxythiophene) (PEDOT), polypyrrole (PPy), and polyaniline (PANI) have excellent stability, high conductivity, and adjustable viscosity [170–174]. They are extensively used for fabricating flexible circuits, sensors, and bio-applications using the inkjet printing technique [175]. In a study, Caironi's group inkjet printed poly (3,4-ethylenedioxythiophene) polystyrene sulfonate (PEDOT:PSS) on a plastic substrate and fabricated an all-polymer field-effect transistor (FET) to operate near field communication (NFC) wireless chip [176,177]. Further Bu et. al. demonstrated inkjet printed FETs using poly(3-hexylthiophene)/polystyrene (P3HT/PS) inks [178].

3.3. Surface matching strategy for printing bio-compatible device on stretchable/bendable substrates

3.3.1. Pretreating the substrate

Since wearable devices need to be flexible and stretchable, they should be fabricated on the substrate materials like Polydimethylsiloxane (PDMS), Thermoplastic polyurethane (TPU), and rubber to achieve the desired flexibility. These materials have low surface energy which implies high contact angle (> 90º) between the ink and the substrate, poor adhesion, and poor wettability [179]. A surface energy mismatch between the ink and the substrates leads to poor ink-substrate interaction, which results in non-uniform ink layer deposition. Nonuniform ink deposition will cause several cracks in the patterns/circuits and further poor conductivity and undesired operation from the patterns/circuits.

To overcome the surface energy mismatch, pretreatment of the substrate has been proposed to increase the surface energy. For example, to enhance the wettability of PDMS, the PDMS substrate surface can be treated with plasma for ~30 sec to 5 min based on the pressure, gas used, and power of the plasma chamber [180–182]. In general, good wetting behavior of the substrate results in a small contact angle (< 90°), while a high contact angle (> 90°) shows poor wetting behavior [183]. Apart from the plasma treatment method, to enhance the adhesion of silver, Wu et. al. proposed a chemical treatment method for the PDMS i.e., treatment of

PDMS with MPTMS (3-mercaptopropyl) trimethoxysilane solution. MPTMS can promote the wettability of the PDMS surface and maintains the adhesion of silver for a usable working time. The resulting printed silver patterns exhibit good compactness and continuity and could be used to fabricate three-electrode electrochemical sensors directly on PDMS [184]. Further, Mikkonen et. al. used a flame pyrolytic surface silicating method, where a thin silicon oxide layer was formed on the substrate surface to significantly improve the adhesion of the conductive inks in comparison to the plasma treatment [185]. However, the wettability of the substrate surface is difficult to control since the surface undergoes "hydrophobic recovery". This "hydrophobic recovery" problem further causes delamination, buckling, mechanical instability, and fracturing of the deposited ink on the substrate in the cyclic loading leading to an irreversible increase in electrical resistances that impede the performance of the printed stretchable circuits [186].

3.3.2. Novel surface matching strategies

Recently many researchers proposed solutions for the challenge of "hydrophobic recovery" during surface treatment by developing novel fabricating strategies. In this section, we will discuss four strategies for successful printing on a stretchable/bendable substrate with their pros and cons and electromechanical performance of printed patterns.

Strategy 1: Pre-stretching the substrate and depositing the conductive material.

Strategy 1 involves stretching the substrate then printing ink on the stretched substrate, and finally releasing the substrate forming an out-of-plane wavy deformation and enhancing the ability of the printed pattern to maintain conductivity under large strain. This stretching process is shown in Figure 8 [187].
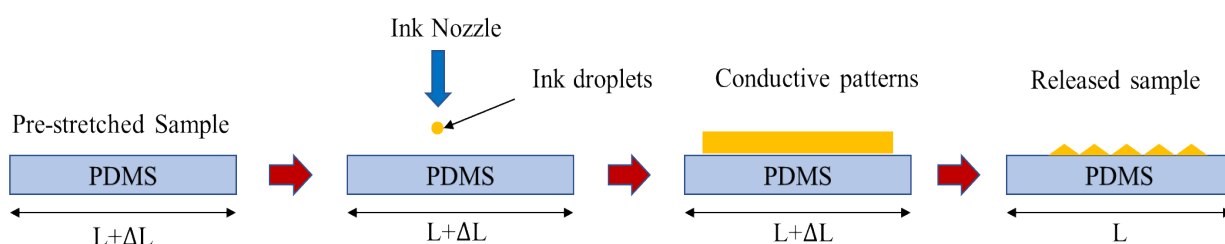
Figure 8. Pre-stretching in axial loading. Reproduced with permission. [187] Copyright 2018, MDPI.

Pre-stretching in axial loading is easy to be applied, however, in most applications, the stretchable sensor was used as a wearable device for health monitoring wherein circuits undergo strain in two directions. Abu-Khalaf et al. [187] introduced radial pre-stretching to improve the performance of the stretchable circuits. The study reveals that radial pre-

stretching increases the out-of-plane deformation compared to axial pre-stretching, hence the radially pre-stretched circuits are more capable to sustain higher radial loads than axially pre-stretched. Figure 9 shows axially and radially stretched PDMS substrate.
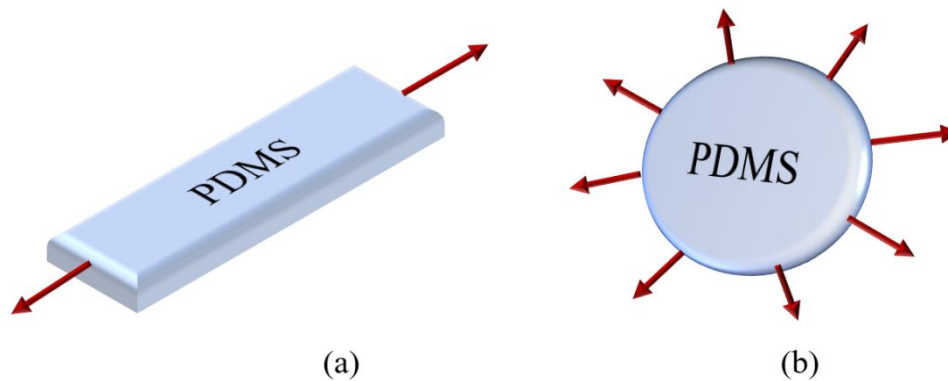

Figure 9. Two pre-stretching methods. (a) Axial pre-stretching. (b) Radial pre-stretching.

The pre-stretching in strategy 1, however, can cause buckling of the electrodes and further the formation of cracks in the lateral direction of pre-stretching due to the Poisson's effect. This effect is caused by strain differences in adjacent materials having different Poisson ratios. To overcome this problem, Lee et. al. proposed an *in-situ* annealing process that causes thermal expansion of PDMS in the direction opposite to that of the Poisson effect, thus compensating for the Poisson's effect. Using this technique, a negligible change was found in resistance - up to a strain of 17% for 1000 stretching cycles [188].

Strategy 2: Printing sinusoidal or horseshoe shape-like patterns on the substrate.

Strategy 2 has a hypothesis that the shapes of the circuits can be designed in such a way that strain on active material will be dissipated by the geometry of the structure during printing. Horseshoe shapes or sinusoidal shapes are widely used because the maximum strain distributed along the meanders of the horseshoe is less than the sharp corners or zigzag shape design [189]. Abu-Khalaf et. al. [111] demonstrated in that this design leads to stable conductivity during stretching. A horseshoe-shaped pattern, printed at an angle of 45° Figure 10 could withstand an axial strain up to 25% with a resistance value of less than 800 Ω. Further, its conductivity could be maintained without any significant changes up to 3000 stretching cycles.

The conductivity performance is also dependent on the mechanical properties of the substrate materials. Plastic deformation can occur in the horseshoe-shaped metal thin film if the magnitude of a local strain exceeds the yielding strain. The plastic deformation accumulated

during cycling will cause the permanent failure of the conductor. Moreover, accumulated shear stress at the metal-substrate interface can cause delamination of the metal film and fail the metal conductivity. Thus, this strategy requires high adhesion between metal film-PDMS substrate for the stable performance of stretchable electronics [189]. To improve the adhesion between film-PDMS, Chung et. al. [190] designed and printed a silver electrode on a wave-structured elastomeric PDMS substrate. UV ozone treated, roughened surface and wavy structure provided a good and stable stretching performance for the printed Ag electrodes. This electrode showed good mechanical stability for 1000 times cycling test under a fast stress-strain test and resistance of the printed electrodes was increased by only 3 times for 30 % tensile strain. This article also reveals that adding a top layer on the wavy PDMS has less change in resistance values as compared to the bare PDMS, this is because of uniform stretching of peak and valley area.
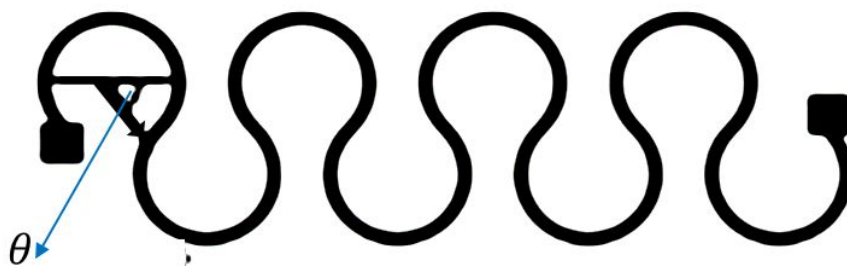

Figure 10. Horseshoe-shaped pattern printed.

Strategy 3: Embedding the conductive material inside the stretchable/bendable substrate.

Strategy 3 has a hypothesis that embedding the conductive material in the liquid elastomer substrate can overcome the issue of "hydrophobic recovery" using surface pretreatment strategies 1 and 2. The focus of this strategy is to print conductive ink into a cross-linkable viscous liquid and restrict the spreading of the ink droplets by encapsulating the ink in a viscous substrate. This method directly embedded the conductive micro cables into the flexible substrate, eliminating the additional step of the encapsulation process. This was achieved by impact force imposed by droplet, match of surface tension between the ink and substrate in liquid form, and quick evaporation of the solvent. Thus, this strategy can avoid hydrophobic recovery, and further reduce delamination, buckling, and fracturing of the deposited conductive material in cyclic loading [186,191]. Jiang et. al. [191] proposed a novel method known as embedded inkjet printing (e-IJP) wherein conductive micro cables are

printed and embedded inside the elastomer substrate. Using this method line width of 1.6 μm and 1.7 aspect ratio were fabricated, which is the highest resolution of conductive lines printed by piezoelectric inkjet printer without any pretreatment. These conductive lines exhibited a negligible increase in resistance for 3000 bending cycles [191].

Further, this research group extended their study by printing semi-wrapped structures to fabricate bendable circuits on pre-cured PDMS. This semi-wrapped circuit was bent to 120° - 150° and a negligible change of resistance was found for 800 bending cycles. This stable conductivity was due to the protection of the encapsulation structure [183].

Similarly, Al-Milaji et. al. [186] printed stretchable conductors by embedding colloidal droplets of silver nanowires (AgNWs) into an uncured liquid PDMS layer by controlling the thickness of the liquid PDMS layer and with a post-printing treatment. The embedding and assembly of the AgNWs consist of three steps (see Figure 11 (b-d)): (1) impact of a droplet in this step, the jetted droplet undergoes droplet−PDMS interactions that prompt the droplet to settle beneath the air-PDMS interface; 2) solvent evaporation and PDMS reflow, helps in directing the assembly of AgNWs; and 3) sinking and deposition of the AgNWs, it streamlines the ink−substrate interactions and positioned the AgNWs in the supporting substrate.
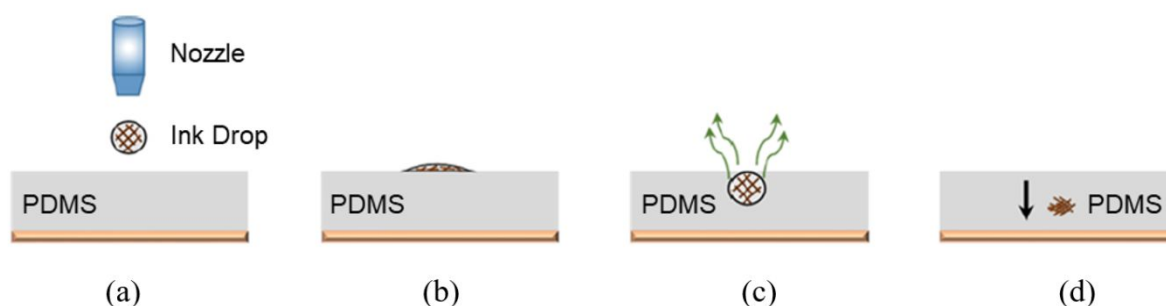

Figure 11. Directly inkjet-printing and embedding AgNWs into an elastomer substrate. (a) Inkjet-printing of AgNWs drop. (b) Droplet impact. (c) Solvent evaporation. (d) Sinking and deposition. Reproduced with permission [186] 2020 American Chemical Society.

Samples fabricated by this technique were stretched for 10% strain for 100 cycles and bent for 150° for 200 cycles and had a negligible change in resistance [186].

Strategy 4: Forming a composite of conductive and stretchable polymer material.

Strategies 1-3 have separate conductive ink material (to be deposited) and the stretchable substrate in printing processes which have problems of surface energy mismatch. The other solution will be mixing ink and substrate material before printing to make a composite stretchable and conductive material. Using an Ag-PDMS composite, Larmagnac et. al. [192] fabricated a stretchable conductor that demonstrated high stretchability i.e. 20% strain over 1000 cycles, and low resistance of 2 Ohm/cm.

Similarly, Woo et. al. used a microcontact printing technique to fabricate a thin artificial skin-like elastomeric capacitive pressure sensor array using a composite material of PDMS and CNT (see Figure 12). These sensor arrays are mechanically robust against stretching, bending, twisting, and folding deformations without any mechanical failures in the sensor structures, such as cracks, fractures, and exfoliation of the elastic conductors. The electrical responses of the devices under repetitive applications of pressure and tensile strain are highly linear, reliable, and reversible. Further, it has negligible dependence on large mechanical deformations for twisting up to 360° [104].
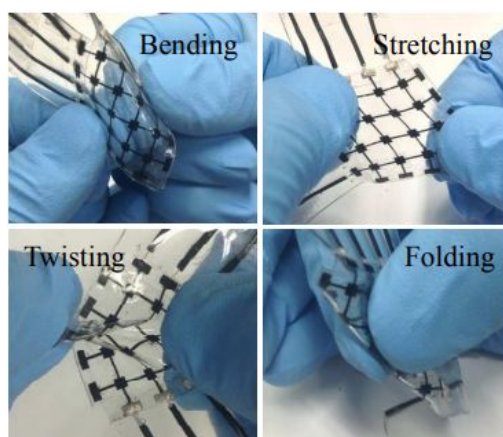

Figure 12. Microcontact printed electrode on PDMS. Reproduced with permission [104]. Copyright 2014, Royal Society of Chemistry.

Claypole et. al. combined carbon black (CB) and ammonia plasma functionalized graphite nanoplatelets (GNPs) in a TPU resin and formulated a conductive ink for stretchable wearables. This ink could be used in screen printing techniques for large-scale manufacturing. Further, it could maintain the electrical conductivity until the breakpoint of approximately 300% nominal strain and cyclic strains of up to 100%. This ink demonstrated a bulk resistivity of 0.196 ±0.013 $\Omega \cdot cm$, similar to the performance of conventional conductive inks [193].

Briefly, the four surface matching strategies are summarized in Table 6 with the highlighted strengths and weaknesses of each strategy. Users can select a strategy for applications according to their requirements.

For wearable FE devices, electromechanical performance under stretching/bending loads is of prime importance. In Table 7 we summarize electromechanical performance achieved by four strategies. More information is provided on the resistance values for the corresponding stretching rate applied to the device/circuits, and percent breakdown strain, for the number of stretching/bending cycles.

Table 6. Pros and cons of surface matching strategies for printing stretchable wearables.

Strategies	Pros	Cons
Strategy 1 [187,188]: • Pre-stretching the substrate	• Optimal performance was achieved by pre-stretching PDMS in axial and radial strain. • Printed circuits withstand repeated stretching cycles and maintained their conductivity without any significant changes. -	• An extra step is needed to find optimum parameters for the surface pre-treatment process. • After surface modification, the contact angle of the ink droplet was enlarged which tends to form line bulges and coalesce into a large droplet, thus reducing the ability to form low-resolution geometry. • Pre stretching and releasing will cause uneven distribution of the stress that may generate cracks. Hence the printed circuits are not robust. Additional encapsulation process required.
Strategy 2 [111,190]: • Printing sinusoidal or horseshoe shape-like pattern on the substrate	• The conductivity of the circuit was fully reversible once it returns to a pre-stretching state. • The printed circuit could withstand repeated stretching cycles and maintained its conductivity without any significant changes. • High-performance stable inkjet printed stretchable electrodes were obtained. • Less change in resistance values was obtained by adding a top layer of PDMS as compared to the circuit fabricated on bare PDMS	• An extra step needed to find optimum parameters for surface pre-treatment process • Printing horseshoe shapes or wavy structures is a painstaking process since it involves optimizing of geometrical parameters like amplitude, line width, the number of cycles and angle to get the best performance. • Horseshoe shape or wavy structure was effective in axial/tensile loading, uncertainty lies regarding their performance in twisting, bending, radial loading, and biaxial loading. • Printed straight line has better stretching performance than horseshoe/wavy shape in radial loading.
Strategy 3 [183,186,191]: • Embedding the conductive material	• No additional surface pretreatment required. • The highest conductive line resolution achieved by inkjet printing without pre-treating substrate.	• Complex fabrication process since coalesces of low-viscosity ink droplets to form straight lines was difficult to control in another liquid. • The use of nanoparticles restricts the performance of the printed

inside the stretchable/bendable substrate during printing	• No additional encapsulation process required. • Stable electrical performance achieved for repeated bending cycles.	circuit to the bending cycle only, however, nanowires can align well during the stretching/bending cycle consequently achieving better performance. • Nanowires are larger (compared to nanoparticles) which may cause clogging of the inkjet printer nozzle.
Strategy 4 [104,192,193]: • Forming a composite of conductive ink and stretchable polymer material	• No surface pretreatment required. • Highly conductive, inexpensive, stretchable inks. • Highly linear, reliable, and reversible electrical performance even when subjected to pressure and tensile strain.	• The high viscosity of the established composite mixture limiting its applications to other printing techniques such as inkjet printing than screen printing, and microcontact printing.

Table 7. Summary of achievable electromechanical performance in the state of the art for various surface matching strategies.

Sr no.	Strategies for printing on Stretchable/Bendable Substrates	Ink Material	Substrate Material	Measured Resistance	Rate of Stretching	Breakdown Strain %	Stretching /Bending Cycle
1a	Pre-stretching the substrate and depositing the conductive material [187,188]	Ag NP	PDMS	40 Ω	Steps of 1 %	19	1000
1b		AgNP	PDMS	6.25 Ω (final)/5.09 Ω (initial)	1mm/min	17	1000
2a	Printing sinusoidal or horseshoe shape like pattern on the substrate [111,190]	AgNP	PDMS	37.0 Ω (final)/13.7 Ω (initial)	1mm/s	10	1000
2b		AgNP	PDMS	800 (f)/100 (i)	Steps of 1 %	25	3000
3a	Fully embedded [183]	AgNP	PDMS	Max= 360 ± 15 Ω	NA	4 mm (bend radius)	
				Negligible			3000 (bending)
3b	Partially embedded (semi wrapped structure) [186]	AgNP	PDMS	Max = 200 ± 10 Ω	NA	120°-150° (bending angle)	
				Negligible	NA		800 (bending)
3c	Fully embedded [191]	AgNW	PDMS	Decrease by 17.1 %	0.2 mm/s	10	100
				Decrease by ~43.2 %	NA	150° (bending angle)	200 (bending)
4a	Forming a composite of conductive and stretchable polymer material [104,192,193]	GNP/CB/ TPU	TPU	55.12% (change in resistance)	50 mm/min	100	20
				1.83%	NA	247 ± 35 N	

						(bending force)	
4b		Ag	PDMS	not given	1mm/s	20	1000
4c		CNT	PDMS	0.25 (change of capacitance)	1 mm/min	50	10
				1 (change of capacitance)	NA	360°(bending angle)	Not provided

Referring to Table 7, all strategies are found promising to a certain extent and application. The third and fourth strategies, however, have a slight edge over the first two because conductive material has been encapsulated by elastomer polymer which eliminates the problem of cracks and wrinkles thus achieving robust printed circuit and better performance. Further, finer resolution lines can be printed. Additionally, no pre-treatment with plasma is required, which eliminates the extra step in the process. Meanwhile, the gaps found in the fabrication techniques for stretchable electronics can be further studied and explored. For instance, the fourth strategy, in addition to screen printing, can also be made suitable for inkjet printing by using an appropriate composition of the conductive material and stretchable elastomer. Design of experiments or machine learning algorithms can be explored for determining the desired ink composition for stretchable electronics.

We comparatively evaluate the electromechanical performance of the four matching strategies for printing FE on stretchable substrates in Table 7. The evaluation measures include resistance values, stretching rate or bending curvature applied to the device/circuits, and corresponding breakdown strain percent, for the number of stretching cycle/bending cycles. It is observed that there is a different approach for calculating resistance values. For instance, 1a and 2b, for corresponding strain, change in resistance was specified as normalized resistance (R_{norm}); R_{norm} = (Final Resistance – Initial resistance)/(Initial resistance), however for 1b and 2a it was defined as R_{norm} = (Resistance measured at specific tensile strain) / (Initial resistance), further rate of application of strain was different, thus comparing R_{norm} values is not justifiable. Third strategies 3a and 3b calculated the change in resistance values for bending only, not specifying any change in resistance values in stretching conditions. It provides maximum resistance values for the corresponding angle/radius of bending and negligible change in resistance for the repeated bending cycle. On the contrary, 3c provided a decrease in resistance upon bending and stretching cycles, which was due to the alignment of AgNWs in the polymer matrix caused by multiple bending and stretching cycles. For strategy 4, we could not find consistent data to compare their performance. Moreover, strategies discussed in Table 7 are mostly unidirectional stretching thus further we can extend our discussion to bidirectional stretching. For instance, Christ et. al. [194] 3D printed a bidirectional strain sensor by integrating multiwalled CNTs into the TPU matrix. They performed testing in various configurations linear axial, linear transverse, linear biaxial, switchback biaxial, and sawtooth biaxial, which resulted in a strain sensor that can withstand a

cyclic loading with strain as high as 50%. In another study, Gao et. al. [195] inkjet-printed a touch sensor by using a "coplanar interlocking diamond shape" pattern which helped to improve touch sensitivity and reduce strain under dynamic deformation. The fabricated sensor could withstand up to 20% dynamic tensile stretching (biaxial tensile stretching). Overall, every article described the methodology suitable for the specific application. Hence, the electromechanical performance of the strategies described in Table 7 cannot be easily compared due to the unavailability of baseline performance metrics. However, it allows us to fill this gap by establishing standard baseline metrics to compare the electromechanical performance of all the manufacturing strategies on a common platform.

4. Scalable Integration of PHC Devices by Inkjet and Other Printing Technologies

Many lab-scale printing processes have been shown to have the capability to print flexible electronics for PHC. However, numerous gaps must be addressed for these printing processes to be scaled up to the industrial scale for the commercialization of low-cost, multifunctional, wearable sensor systems for PHC. The research and development gaps for emerging sensor platforms span over a range of interdisciplinary, vertically integrated designs and processes to realize the sensors, wireless communication, data acquisition, manufacturing, and material technologies, combined with specific biosensing expertise. To address these challenges, novel bio, chemical, electronic, and nanomaterial-enabled sensor platforms are being developed using low-cost manufacturing capability. Such sensor platforms must increase the level of intelligence and data collection utilizing designs, implementing low-power, wireless networking, onboard signal processing, memory, energy harvesting, and optimal form factor. Furthermore, evaluation and test must be conducted in controlled but highly realistic conditions, accounting for human interaction, and including informatics to accurately inform on health care conditions. As illustrated in Figure 13, scalable fabrication methods for the measurement of stress/fatigue biomarkers from sweat have been developed using inkjet-printed electronics integrated with imprinted microfluidic devices [69,196]. This approach demonstrated a lab-scale adhesive sensor patch for monitoring sweat electrolytes — collecting sweat and measuring biomarkers, such as glucose or cortisol, and reporting the data using an integrated RFID antenna for near-field communications readout. This approach does not utilize complex system designs that require controllers or active component integration. As illustrated in Figure 13, the next level of

integration would incorporate more complex designs and circuit elements that enable arrays of microfluidic channels to be realized, each with biosensing elements, microfluidic sample control, and data readout [197]. They will be fabricated via advanced printing techniques (e.g. inkjet printing and nanoimprinting) scalable to continuous fabrication processes. This example of a wearable patch is capable of measuring cortisol (or other potential biomarkers utilizing specific antibodies) that are acquired from sweat via absorbing pads, along with integrated capillary microfluidic channels and opening valves. An electronic sensor decorated with cortisol antibody will measure the cortisol concentration and transfer the data via wireless connection for personnel health evaluation. Ultimately, the progression for a fully printed microfluidic sensor solution will include energy harvesting, basic sensing function, data communication, and hybrid integration of electronic signal processing [198–201].
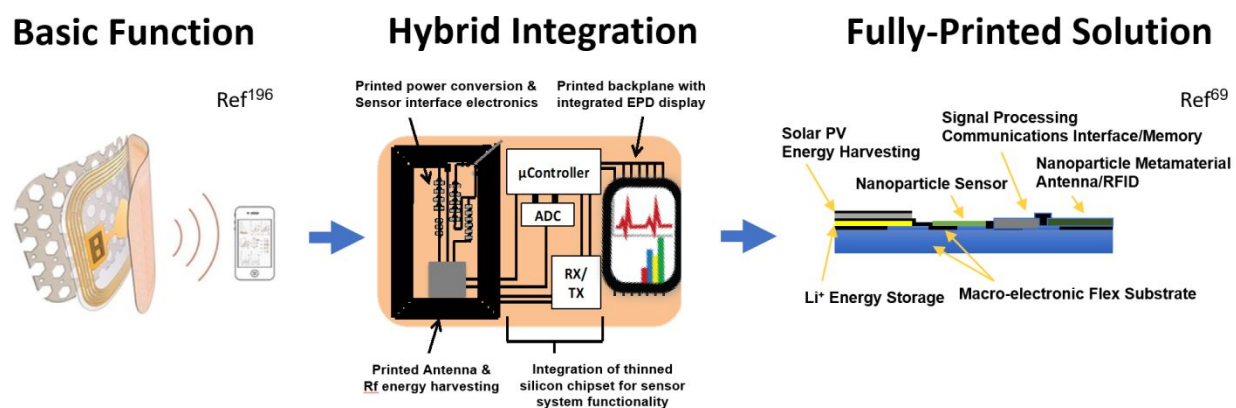

Figure 13. Technology progression for flexible patch sensors. Reproduced with permission [196]. Copyright 2015, The Boston globe. Reproduced with permission [69]. Copyright 2014.

Examples of such integrated sweat collection devices and systems include inkjet printing of electrodes and opening valves, nanoimprinting of microfluidic channels, and flexible substrate integration have been developed toward a fully integrated sweat sensing system. As shown in Figure 14, [49,201] a sweat patch was designed in multiple layers incorporating inkjet and nanoimprinting processes, which include inkjet-printed basic electrochemical sensing function, along with inkjet-printed electrowetting valves in the microfluidic channels to control the flow of samples collected. In this example, a flexible microfluidic chip is formed potentially scalable to R2R processing for high-throughput and low-cost fabrication [49].
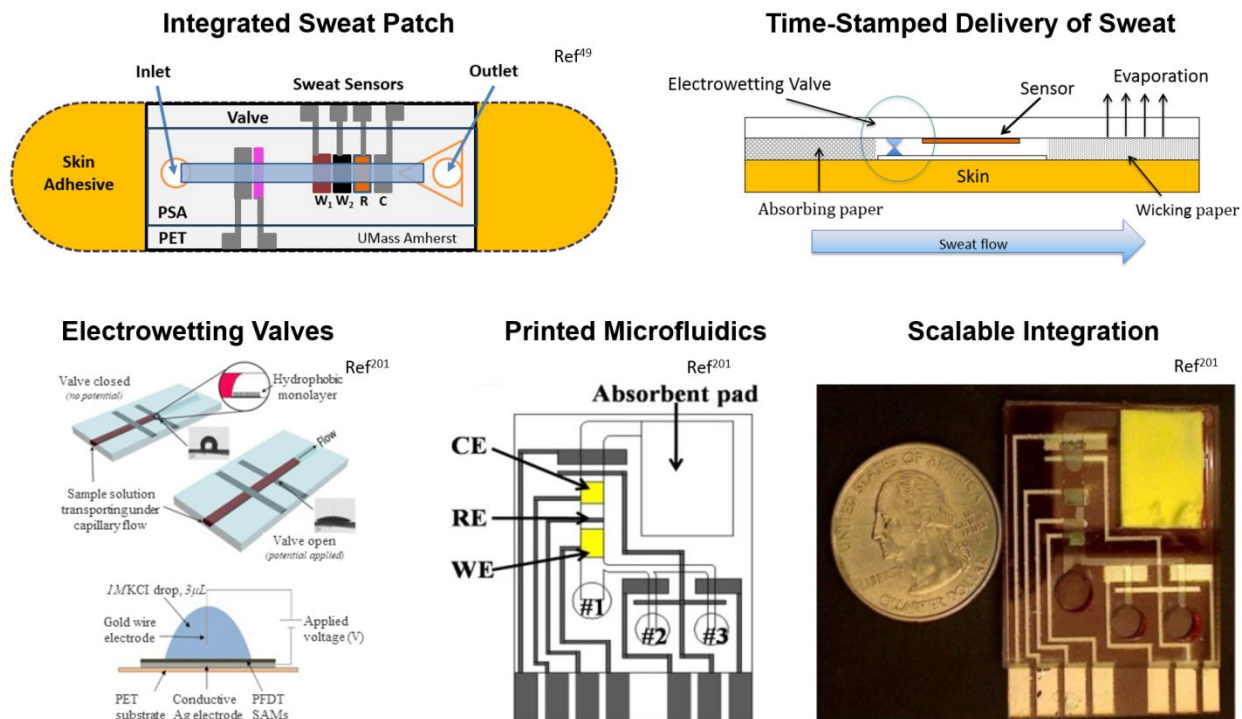
Figure 14. Integrated functional microfluidics designed for and printed by inkjet printing of electrodes and nanoimprinting Reproduced with permission [49]. Copyright 2019. Reproduced with permission [201]. Copyright 2016, IEEE.

5. Conclusions and Future Perspectives

This article reviews and provides insight into distinct types of wearable devices used for PHM designed and developed by researchers in academia and industry. It tries to bridge the gap between the wearable FE for PHC and the corresponding fabricating techniques applied in this research. Various fabrication techniques for these devices with a deep analysis of their pros, cons, and applications were introduced.   Wearable FE for PHC was classified into vitals monitoring and medical aid wearable devices, further, printing technologies, substrates, and ink materials used for these devices were summarized. Inkjet printing technologies were identified as a potential fabrication technique having a vast scope for manufacturing wearable devices; mainly because of its numerous advantages, non-contact type printing process, mask-free printing, highly customizable with digital control patterning, it a lean and clean process i.e., it does not produce much waste, and compatible with various substrates. Several examples of inkjet-printed wearable PHC devices like Respiratory Rate (RR) sensors, temperature sensors, heart rate, arterial oxygen saturation (SpO2) sensors, antenna for wearable tracking devices, etc. with their performance were highlighted. Moreover, the mechanism of inkjet printing with various

parameters and ink formulation required for printing on the flexible substrate were discussed. Further, four surface matching strategies used for printing PHC stretchable devices, highlighting their pros and cons, and a comparison of the electromechanical performance along with the functional material and the substrate were discussed. Fabrication of the wearable FE for PHC using inkjet printing has recently caught the attention of many researchers and substantial progress has been made. Though significant contributions have been made, there are some challenges need to be addressed that create an equal number of opportunities for the future.

Most of the strategies discussed in the literature are restricted to a single substrate (e.g., PDMS). A single process can be developed for printing on multiple substrates, while we need to consider the relationship between the surface energy of the substrate, the surface tension of the ink to be deposited, and its effect on the conductivity of the final printed pattern. Strategies to print on the stretchable substrates are difficult to comparatively evaluate concerning their electro-mechanical performance, however, we can develop a common matrix to measure their performance to find the best fit. Environment, society, and economics are the three pillars of sustainability defined by the US Environmental Protection Agency [202], articles discussing on printing of wearable device lacks this focus to some extent, although PDMS used in most of the devices is biodegradable; recycling, remanufacturing, life cycle analysis (LCA) of the printed wearable devices is the area which needs to be explored. Quality, cost, and time are three governing factors of a product development industry. In the near future, demand for high-quality, low-cost, and large-scale production in a limited amount of time will impact the PHM device manufacturing sector. To meet such a demand, we need a synergistic manufacturing system that will combine the advantages of multiple manufacturing techniques and produce the best possible output. For instance, an amalgamation of contact and non-contact printing i.e., μCP and inkjet printing can be blended into an R2R system which would combine the benefits of both manufacturing techniques i.e., high resolution and agility of the μCP and versatility of inkjet printing techniques. This can be followed by other print methods like screen printing or flexography to produce the best possible outcome. Further, a study depicting, a model of such a manufacturing system should be developed and tested. In general, for wearable devices, multifunction, integration, and flexibility are important and can further be explored.

Author contributions

X.D. conceived the idea and supervised the survey. X.D., S.W., S.P., and J.M. wrote the manuscript. X.D., S.W., A.S., and N.L. prepared all the figures and tables. All authors reviewed the manuscript and provided corrections and comments.

Acknowledgment

Conflict of Interest

References

1   J. O'Donoghue, J. Herbert and P. Stack, Remote Non-Intrusive Patient Monitoring, 8.

2   S. Khan, S. Ali and A. Bermak, Recent Developments in Printing Flexible and Wearable Sensing Electronics for Healthcare Applications, *Sensors (Basel)*, , DOI:10.3390/s19051230.

3   R. Humbare, S. Wankhede and V. Kumar, Flexible Electronics Market Size, Share & Growth | Analysis - 2027, https://www.alliedmarketresearch.com/flexible-electronics-market, (accessed 23 January 2022).

4   Global Flexible Display Market Reports, Market Share, Market Analysis, Market Trends and Forecast 2017 - 2023, https://www.occamsresearch.com/flexible-display-market/, (accessed 23 May 2021).

5   C. M. Boutry, L. Beker, Y. Kaizawa, C. Vassos, H. Tran, A. C. Hinckley, R. Pfattner, S. Niu, J. Li, J. Claverie, Z. Wang, J. Chang, P. M. Fox and Z. Bao, Biodegradable and flexible arterial-pulse sensor for the wireless monitoring of blood flow, *Nature Biomedical Engineering*, 2019, **3**, 47–57.

6   A. Singh, B. J. Wakefield and A. E. Duncan, Complications from brachial arterial pressure monitoring are rare in patients having cardiac surgery, *J Thorac Dis*, 2018, **10**, E158–E159.

7   PyrAmes, https://pyrameshealth.com/, (accessed 23 May 2021).

8   Biosensor BX100 Wearable biosensor | Philips Healthcare, https://www.usa.philips.com/healthcare/product/HC989803203011/biosensor-bx100-wearable-biosensor, (accessed 23 May 2021).

9   K. Sim, Z. Rao, Z. Zou, F. Ershad, J. Lei, A. Thukral, J. Chen, Q.-A. Huang, J. Xiao and C. Yu, Metal oxide semiconductor nanomembrane–based soft unnoticeable multifunctional electronics for wearable human-machine interfaces, *Science Advances*, 2019, **5**, eaav9653.

10   Y. Yamamoto, S. Harada, D. Yamamoto, W. Honda, T. Arie, S. Akita and K. Takei, Printed multifunctional flexible device with an integrated motion sensor for health care monitoring, *Science Advances*, 2016, **2**, e1601473.

11   Vivalink, Vivalink, https://www.vivalink.com, (accessed 23 May 2021).

12   Masimo, https://www.masimo.com/healthcare/, (accessed 23 May 2021).

13   Solos Analytics, https://www.solosanalytics.com/, (accessed 23 May 2021).

14   J. Viventi, D.-H. Kim, J. D. Moss, Y.-S. Kim, J. A. Blanco, N. Annetta, A. Hicks, J. Xiao, Y. Huang, D. J. Callans, J. A. Rogers and B. Litt, A Conformal, Bio-Interfaced Class of Silicon Electronics for Mapping Cardiac Electrophysiology, *Science Translational Medicine*, 2010, **2**, 24ra22-24ra22.

15   Sure Pulse Medical, https://www.surepulsemedical.com/, (accessed 24 May 2021).

16   C. M. Lochner, Y. Khan, A. Pierre and A. C. Arias, All-organic optoelectronic sensor for pulse oximetry, *Nature Communications*, 2014, **5**, 5745.

17   Y. Khan, D. Han, A. Pierre, J. Ting, X. Wang, C. M. Lochner, G. Bovo, N. Yaacobi-Gross, C. Newsome, R. Wilson and A. C. Arias, A flexible organic reflectance oximeter array, *PNAS*, 2018, **115**, E11015–E11024.

18   J. Kim, P. Gutruf, A. M. Chiarelli, S. Y. Heo, K. Cho, Z. Xie, A. Banks, S. Han, K.-I. Jang, J. W. Lee, K.-T. Lee, X. Feng, Y. Huang, M. Fabiani, G. Gratton, U. Paik and J. A. Rogers, Miniaturized Battery-Free Wireless Systems for Wearable Pulse Oximetry, *Adv Funct Mater*, , DOI:10.1002/adfm.201604373.

19   R. C. Webb, Y. Ma, S. Krishnan, Y. Li, S. Yoon, X. Guo, X. Feng, Y. Shi, M. Seidel, N. H. Cho, J. Kurniawan, J. Ahad, N. Sheth, J. Kim, J. G. T. Vi, T. Darlington, K. Chang, W. Huang, J. Ayers, A. Gruebele, R. M. Pielak, M. J. Slepian, Y. Huang, A. M. Gorbach and J. A. Rogers, Epidermal devices for noninvasive, precise, and continuous mapping of macrovascular and microvascular blood flow, *Science Advances*, 2015, **1**, e1500701.

20 S. R. Krishnan, T. R. Ray, A. B. Ayer, Y. Ma, P. Gutruf, K. Lee, J. Y. Lee, C. Wei, X. Feng, B. Ng, Z. A. Abecassis, N. Murthy, I. Stankiewicz, J. Freudman, J. Stillman, N. Kim, G. Young, C. Goudeseune, J. Ciraldo, M. Tate, Y. Huang, M. Potts and J. A. Rogers, Epidermal electronics for noninvasive, wireless, quantitative assessment of ventricular shunt function in patients with hydrocephalus, *Science Translational Medicine*, , DOI:10.1126/scitranslmed.aat8437.

21 G. Cai, J. Wang, K. Qian, J. Chen, S. Li and P. S. Lee, Extremely Stretchable Strain Sensors Based on Conductive Self-Healing Dynamic Cross-Links Hydrogels for Human-Motion Detection, *Advanced Science*, 2017, **4**, 1600190.

22 CurveSYS, https://curvesys.de/en/, (accessed 23 May 2021).

23 Tacterion - plyon® Sensor Technology, https://www.tacterion.com/, (accessed 23 May 2021).

24 Bend Labs, https://www.bendlabs.com/, (accessed 23 May 2021).

25 Z. Lin, J. Chen, X. Li, Z. Zhou, K. Meng, W. Wei, J. Yang and Z. L. Wang, Triboelectric Nanogenerator Enabled Body Sensor Network for Self-Powered Human Heart-Rate Monitoring, *ACS Nano*, 2017, **11**, 8830–8837.

26 A. Alizadeh, A. Burns, R. Lenigk, R. Gettings, J. Ashe, A. Porter, M. McCaul, R. Barrett, D. Diamond, P. White, P. Skeath and M. Tomczak, A wearable patch for continuous monitoring of sweat electrolytes during exertion, *Lab Chip*, 2018, **18**, 2632–2641.

27 J. Choi, R. Ghaffari, L. B. Baker and J. A. Rogers, Skin-interfaced systems for sweat collection and analytics, *Sci. Adv.*, 2018, **4**, eaar3921.

28 Y. Zhao, B. Wang, H. Hojaiji, Z. Wang, S. Lin, C. Yeung, H. Lin, P. Nguyen, K. Chiu, K. Salahi, X. Cheng, J. Tan, B. A. Cerrillos and S. Emaminejad, A wearable freestanding electrochemical sensing system, *Science Advances*, 2020, **6**, eaaz0007.

29 J. T. Reeder, J. Choi, Y. Xue, P. Gutruf, J. Hanson, M. Liu, T. Ray, A. J. Bandodkar, R. Avila, W. Xia, S. Krishnan, S. Xu, K. Barnes, M. Pahnke, R. Ghaffari, Y. Huang and J. A. Rogers, Waterproof, electronics-enabled, epidermal microfluidic devices for sweat collection, biomarker analysis, and thermography in aquatic settings, *Science Advances*, 2019, **5**, eaau6356.

30 Y. Liu, J. J. S. Norton, R. Qazi, Z. Zou, K. R. Ammann, H. Liu, L. Yan, P. L. Tran, K.-I. Jang, J. W. Lee, D. Zhang, K. A. Kilian, S. H. Jung, T. Bretl, J. Xiao, M. J. Slepian, Y.

Huang, J.-W. Jeong and J. A. Rogers, Epidermal mechano-acoustic sensing electronics for cardiovascular diagnostics and human-machine interfaces, *Science Advances*, 2016, **2**, e1601185.

31 J. Kim, J. R. Sempionatto, S. Imani, M. C. Hartel, A. Barfidokht, G. Tang, A. S. Campbell, P. P. Mercier and J. Wang, Simultaneous Monitoring of Sweat and Interstitial Fluid Using a Single Wearable Biosensor Platform, *Adv Sci (Weinh)*, , DOI:10.1002/advs.201800880.

32 H. Lee, T. K. Choi, Y. B. Lee, H. R. Cho, R. Ghaffari, L. Wang, H. J. Choi, T. D. Chung, N. Lu, T. Hyeon, S. H. Choi and D.-H. Kim, A graphene-based electrochemical device with thermoresponsive microneedles for diabetes monitoring and therapy, *Nature Nanotechnology*, 2016, **11**, 566–572.

33 W. Gao, S. Emaminejad, H. Y. Y. Nyein, S. Challa, K. Chen, A. Peck, H. M. Fahad, H. Ota, H. Shiraki, D. Kiriya, D.-H. Lien, G. A. Brooks, R. W. Davis and A. Javey, Fully integrated wearable sensor arrays for multiplexed in situ perspiration analysis, *Nature*, 2016, **529**, 509–514.

34 M. A. Howard, R. Asmis, K. K. Evans and T. A. Mustoe, Oxygen and wound care: a review of current therapeutic modalities and future direction, *Wound Repair Regen*, 2013, **21**, 503–511.

35 M. Ochoa, R. Rahimi, J. Zhou, H. Jiang, C. K. Yoon, M. Oscai, V. Jain, T. Morken, R. H. Oliveira, D. Maddipatla, B. B. Narakathu, G. L. Campana, M. A. Zieger, R. Sood, M. Z. Atashbar and B. Ziaie, in *Micro- and Nanotechnology Sensors, Systems, and Applications X*, International Society for Optics and Photonics, 2018, vol. 10639, p. 106391C.

36 Nemera, https://www.nemera.net/, (accessed 24 May 2021).

37 Neuralink, https://neuralink.com/, (accessed 24 May 2021).

38 Y. Zhang, N. Zheng, Y. Cao, F. Wang, P. Wang, Y. Ma, B. Lu, G. Hou, Z. Fang, Z. Liang, M. Yue, Y. Li, Y. Chen, J. Fu, J. Wu, T. Xie and X. Feng, Climbing-inspired twining electrodes using shape memory for peripheral nerve stimulation and recording, *Science Advances*, 2019, **5**, eaaw1066.

39 C. Lu, S. Park, T. J. Richner, A. Derry, I. Brown, C. Hou, S. Rao, J. Kang, C. T. Mortiz, Y. Fink and P. Anikeeva, Flexible and stretchable nanowire-coated fibers for optoelectronic probing of spinal cord circuits, *Sci. Adv.*, 2017, **3**, e1600955.

40 S.-H. Byun, J. Y. Sim, Z. Zhou, J. Lee, R. Qazi, M. C. Walicki, K. E. Parker, M. P. Haney, S. H. Choi, A. Shon, G. B. Gereau, J. Bilbily, S. Li, Y. Liu, W.-H. Yeo, J. G. McCall, J. Xiao and J.-W. Jeong, Mechanically transformative electronics, sensors, and implantable devices, *Sci. Adv.*, 2019, **5**, eaay0418.

41 T. Cramer, I. Fratelli, P. Barquinha, A. Santa, C. Fernandes, F. D'Annunzio, C. Loussert, R. Martins, E. Fortunato and B. Fraboni, Passive radiofrequency x-ray dosimeter tag based on flexible radiation-sensitive oxide field-effect transistor, *Sci. Adv.*, 2018, **4**, eaat1825.

42 S. Y. Heo, J. Kim, P. Gutruf, A. Banks, P. Wei, R. Pielak, G. Balooch, Y. Shi, H. Araki, D. Rollo, C. Gaede, M. Patel, J. W. Kwak, A. E. Peña-Alcántara, K.-T. Lee, Y. Yun, J. K. Robinson, S. Xu and J. A. Rogers, Wireless, battery-free, flexible, miniaturized dosimeters monitor exposure to solar radiation and to light for phototherapy, *Science Translational Medicine*, , DOI:10.1126/scitranslmed.aau1643.

43 Y. Wu, Y. Liu, Y. Zhou, Q. Man, C. Hu, W. Asghar, F. Li, Z. Yu, J. Shang, G. Liu, M. Liao and R.-W. Li, A skin-inspired tactile sensor for smart prosthetics, *Science Robotics*, , DOI:10.1126/scirobotics.aat0429.

44 B. C.-K. Tee, A. Chortos, A. Berndt, A. K. Nguyen, A. Tom, A. McGuire, Z. C. Lin, K. Tien, W.-G. Bae, H. Wang, P. Mei, H.-H. Chou, B. Cui, K. Deisseroth, T. N. Ng and Z. Bao, A skin-inspired organic digital mechanoreceptor, *Science*, 2015, **350**, 313–316.

45 A. J. Bandodkar, C. S. López, A. M. V. Mohan, L. Yin, R. Kumar and J. Wang, All-printed magnetically self-healing electrochemical devices, *Science Advances*, 2016, **2**, e1601465.

46 S. Mishra, Y.-S. Kim, J. Intarasirisawat, Y.-T. Kwon, Y. Lee, M. Mahmood, H.-R. Lim, R. Herbert, K. J. Yu, C. S. Ang and W.-H. Yeo, Soft, wireless periocular wearable electronics for real-time detection of eye vergence in a virtual reality toward mobile eye therapies, *Science Advances*, 2020, **6**, eaay1729.

47 X. Shi, Z.-S. Wu and X. Bao, Recent Advancements and Perspective of High-Performance Printed Power Sources with Multiple Form Factors, *Electrochem. Energ. Rev.*, 2020, **3**, 581–612.

48 Z. Wen, M.-H. Yeh, H. Guo, J. Wang, Y. Zi, W. Xu, J. Deng, L. Zhu, X. Wang, C. Hu, L. Zhu, X. Sun and Z. L. Wang, Self-powered textile for wearable electronics by hybridizing fiber-shaped nanogenerators, solar cells, and supercapacitors, *Science Advances*, 2016, **2**, e1600097.

49 Y. Zhou, University of Massachusetts Amherst.

50 R. Abbel, P. Teunissen, E. Rubingh, T. van Lammeren, R. Cauchois, M. Everaars, J. Valeton, S. van de Geijn and P. Groen, Industrial-scale inkjet printed electronics manufacturing—production up-scaling from concept tools to a roll-to-roll pilot line, *Transl. Mater. Res.*, 2014, **1**, 015002.

51 S. Khan, L. Lorenzelli and R. S. Dahiya, Technologies for Printing Sensors and Electronics Over Large Flexible Substrates: A Review, *IEEE Sensors J.*, 2015, **15**, 3164–3185.

52 V. Sanchez-Romaguera, M. A. Ziai, D. Oyeka, S. Barbosa, J. S. R. Wheeler, J. C. Batchelor, E. A. Parker and S. G. Yeates, Towards inkjet-printed low cost passive UHF RFID skin mounted tattoo paper tags based on silver nanoparticle inks, *J. Mater. Chem. C*, 2013, **1**, 6395–6402.

53 D. Angmo, T. T. Larsen-Olsen, M. Jørgensen, R. R. Søndergaard and F. C. Krebs, Roll-to-Roll Inkjet Printing and Photonic Sintering of Electrodes for ITO Free Polymer Solar Cell Modules and Facile Product Integration, *Advanced Energy Materials*, 2013, **3**, 172–175.

54 K. Y. Mitra, S. Kapadia, M. Hartwig, E. Sowade, Z. Xu, R. R. Baumann and R. Zichner, in *NIP & Digital Fabrication Conference*, Society for Imaging Science and Technology, 2018, vol. 2018, pp. 21–32.

55 W.-Y. Chang, T.-H. Fang, H.-J. Lin, Y.-T. Shen and Y.-C. Lin, A Large Area Flexible Array Sensors Using Screen Printing Technology, *J. Display Technol., JDT*, 2009, **5**, 178–183.

56 D. Numakura, in *2008 3rd International Microsystems, Packaging, Assembly Circuits Technology Conference*, 2008, pp. 205–208.

57 W. J. Hyun, E. B. Secor, M. C. Hersam, C. D. Frisbie and L. F. Francis, High-Resolution Patterning of Graphene by Screen Printing with a Silicon Stencil for Highly Flexible Printed Electronics, *Advanced Materials*, 2015, **27**, 109–115.

58 J. Szlufcik, F. Duerinckx, J. Horzel, E. Van Kerschaver, H. Dekkers, S. De Wolf, P. Choulat, C. Allebe and J. Nijs, High-efficiency low-cost integral screen-printing multicrystalline silicon solar cells, *Solar Energy Materials and Solar Cells*, 2002, **74**, 155–163.

59 MURAKAMI CO., LTD., https://www.murakami.co.jp/english/about/index.html, (accessed 25 May 2021).

60 X. Cao, H. Chen, X. Gu, B. Liu, W. Wang, Y. Cao, F. Wu and C. Zhou, Screen Printing as a Scalable and Low-Cost Approach for Rigid and Flexible Thin-Film Transistors Using Separated Carbon Nanotubes, *ACS Nano*, 2014, **8**, 12769–12776.

61 Luminite, Flexo Printing vs Gravure Printing, https://blog.luminite.com/blog/flexo-printing-vs-gravure-printing, (accessed 25 May 2021).

62 E. B. Secor, S. Lim, H. Zhang, C. D. Frisbie, L. F. Francis and M. C. Hersam, Gravure printing of graphene for large-area flexible electronics, *Adv Mater*, 2014, **26**, 4533–4538.

63 S. Kim, H. Sojoudi, H. Zhao, D. Mariappan, G. H. McKinley, K. K. Gleason and A. J. Hart, Ultrathin high-resolution flexographic printing using nanoporous stamps, *Science Advances*, 2016, **2**, e1601660.

64 J. Benson, C. M. Fung, J. S. Lloyd, D. Deganello, N. A. Smith and K. S. Teng, Direct patterning of gold nanoparticles using flexographic printing for biosensing applications, *Nanoscale Research Letters*, 2015, **10**, 127.

65 C. Wang, C. Linghu, S. Nie, C. Li, Q. Lei, X. Tao, Y. Zeng, Y. Du, S. Zhang, K. Yu, H. Jin, W. Chen and J. Song, Programmable and scalable transfer printing with high reliability and efficiency for flexible inorganic electronics, *Science Advances*, 2020, **6**, eabb2393.

66 C. Zhang, C.-L. Zou, Y. Zhao, C.-H. Dong, C. Wei, H. Wang, Y. Liu, G.-C. Guo, J. Yao and Y. S. Zhao, Organic printed photonics: From microring lasers to integrated circuits, *Science Advances*, 2015, **1**, e1500257.

67 C. Wang, D. B. Collins, C. Arata, A. H. Goldstein, J. M. Mattila, D. K. Farmer, L. Ampollini, P. F. DeCarlo, A. Novoselac, M. E. Vance, W. W. Nazaroff and J. P. D. Abbatt, Surface reservoirs dominate dynamic gas-surface partitioning of many indoor air constituents, *Science Advances*, 2020, **6**, eaay8973.

68 N. Kooy, K. Mohamed, L. T. Pin and O. S. Guan, A review of roll-to-roll nanoimprint lithography, *Nanoscale Res Lett*, 2014, **9**, 320.

69 J. Morse, Advanced Nanomanufacturing for Wearable Human Performance Monitoring Sensor Platforms, , DOI:10.13028/1C7E-XQ92.

70 E. Cho, M. Mohammadifar and S. Choi, A Single-Use, Self-Powered, Paper-Based Sensor Patch for Detection of Exercise-Induced Hypoglycemia, *Micromachines*, 2017, **8**, 265.

71 A. Koh, D. Kang, Y. Xue, S. Lee, R. M. Pielak, J. Kim, T. Hwang, S. Min, A. Banks, P. Bastien, M. C. Manco, L. Wang, K. R. Ammann, K.-I. Jang, P. Won, S. Han, R. Ghaffari, U.

Paik, M. J. Slepian, G. Balooch, Y. Huang and J. A. Rogers, A soft, wearable microfluidic device for the capture, storage, and colorimetric sensing of sweat, *Science Translational Medicine*, 2016, **8**, 366ra165-366ra165.

72 S. Emaminejad, W. Gao, E. Wu, Z. A. Davies, H. Yin Yin Nyein, S. Challa, S. P. Ryan, H. M. Fahad, K. Chen, Z. Shahpar, S. Talebi, C. Milla, A. Javey and R. W. Davis, Autonomous sweat extraction and analysis applied to cystic fibrosis and glucose monitoring using a fully integrated wearable platform, *Proceedings of the National Academy of Sciences*, 2017, **114**, 4625–4630.

73 J. Li, F. Rossignol and J. Macdonald, Inkjet printing for biosensor fabrication: combining chemistry and technology for advanced manufacturing, *Lab Chip*, 2015, **15**, 2538–2558.

74 M. Gao, L. Li and Y. Song, Inkjet printing wearable electronic devices, *J. Mater. Chem. C*, 2017, **5**, 2971–2993.

75 W. Gao, H. Ota, D. Kiriya, K. Takei and A. Javey, Flexible Electronics toward Wearable Sensing, *Acc. Chem. Res.*, 2019, **52**, 523–533.

76 S. P. Sreenilayam, I. U. Ahad, V. Nicolosi, V. Acinas Garzon and D. Brabazon, Advanced materials of printed wearables for physiological parameter monitoring, *Materials Today*, 2020, **32**, 147–177.

77 Y. Zhang, G. Shi, J. Qin, S. E. Lowe, S. Zhang, H. Zhao and Y. L. Zhong, Recent Progress of Direct Ink Writing of Electronic Components for Advanced Wearable Devices, *ACS Appl. Electron. Mater.*, 2019, **1**, 1718–1734.

78 S. Shrivastava, T. Quang Trung and N.-E. Lee, Recent progress, challenges, and prospects of fully integrated mobile and wearable point-of-care testing systems for self-testing, *Chemical Society Reviews*, 2020, **49**, 1812–1866.

79 D. Maddipatla, B. B. Narakathu and M. Atashbar, Recent Progress in Manufacturing Techniques of Printed and Flexible Sensors: A Review, *Biosensors (Basel)*, 2020, **10**, E199.

80 K. Yan, J. Li, L. Pan and Y. Shi, Inkjet printing for flexible and wearable electronics, *APL Materials*, 2020, **8**, 120705.

81 S. M. A. Iqbal, I. Mahgoub, E. Du, M. A. Leavitt and W. Asghar, Advances in healthcare wearable devices, *npj Flex Electron*, 2021, **5**, 1–14.

82 C. Demolder, A. Molina, F. L. Hammond and W.-H. Yeo, Recent advances in wearable biosensing gloves and sensory feedback biosystems for enhancing rehabilitation, prostheses, healthcare, and virtual reality, *Biosensors and Bioelectronics*, 2021, **190**, 113443.

83 J. Suikkola, T. Björninen, M. Mosallaei, T. Kankkunen, P. Iso-Ketola, L. Ukkonen, J. Vanhala and M. Mäntysalo, Screen-Printing Fabrication and Characterization of Stretchable Electronics, *Sci Rep*, 2016, **6**, 25784.

84 A. Nathan, A. Ahnood, M. Cole, S. Lee, Y. Suzuki, P. Hiralal, F. Bonaccorso, T. Hasan, L. Garcia-Gancedo, A. Dyadyusha, S. Haque, P. Andrew, S. Hofmann, J. Moultrie, D. Chu, A. J. Flewitt, A. C. Ferrari, M. J. Kelly, J. Robertson, G. A. J. Amaratunga and W. I. Milne, Flexible electronics: The next ubiquitous platform, *Proceedings of the IEEE*, 2012, **100**, 1486–1517.

85 R. F. Pease and S. Y. Chou, Lithography and Other Patterning Techniques for Future Electronics, *Proceedings of the IEEE*, 2008, **96**, 248–270.

86 R. R. Søndergaard, M. Hösel and F. C. Krebs, Roll-to-Roll fabrication of large area functional organic materials, *Journal of Polymer Science Part B: Polymer Physics*, 2013, **51**, 16–34.

87 D. Tobjörk and R. Österbacka, Paper Electronics, *Advanced Materials*, 2011, **23**, 1935–1961.

88 M. A. M. Leenen, V. Arning, H. Thiem, J. Steiger and R. Anselmann, Printable electronics: flexibility for the future, *physica status solidi (a)*, 2009, **206**, 588–597.

89 V. Subramanian, J. B. Chang, A. de la Fuente Vornbrock, D. C. Huang, L. Jagannathan, F. Liao, B. Mattis, S. Molesa, D. R. Redinger, D. Soltman, S. K. Volkman and Q. Zhang, in *ESSCIRC 2008 - 34th European Solid-State Circuits Conference*, 2008, pp. 17–24.

90 P. F. Moonen, I. Yakimets and J. Huskens, Fabrication of transistors on flexible substrates: from mass-printing to high-resolution alternative lithography strategies, *Adv Mater*, 2012, **24**, 5526–5541.

91 D. Wang, Y. Zhang, X. Lu, Z. Ma, C. Xie and Z. Zheng, Chemical formation of soft metal electrodes for flexible and wearable electronics, *Chem. Soc. Rev.*, 2018, **47**, 4611–4641.

92 T. Someya, T. Sekitani, S. Iba, Y. Kato, H. Kawaguchi and T. Sakurai, A large-area, flexible pressure sensor matrix with organic field-effect transistors for artificial skin applications, *PNAS*, 2004, **101**, 9966–9970.

93 S. Harada, K. Kanao, Y. Yamamoto, T. Arie, S. Akita and K. Takei, Fully printed flexible fingerprint-like three-axis tactile and slip force and temperature sensors for artificial skin, *ACS Nano*, 2014, **8**, 12851–12857.

94 D. Ji, Z. Shi, Z. Liu, S. S. Low, J. Zhu, T. Zhang, Z. Chen, X. Yu, Y. Lu, D. Lu and Q. Liu, Smartphone-based square wave voltammetry system with screen-printed graphene electrodes for norepinephrine detection, *Smart Materials in Medicine*, 2020, **1**, 1–9.

95 D. C. Han, H. J. Shin, S. Yeom and W. Lee, Wearable Human Health-monitoring Band using Inkjet-printed Flexible Temperature Sensor, 2017, **26**, 301–305.

96 M. Choi, Y. J. Park, B. K. Sharma, S.-R. Bae, S. Y. Kim and J.-H. Ahn, Flexible active-matrix organic light-emitting diode display enabled by MoS2 thin-film transistor, *Science Advances*, 2018, **4**, eaas8721.

97 R. Shiwaku, H. Matsui, K. Nagamine, M. Uematsu, T. Mano, Y. Maruyama, A. Nomura, K. Tsuchiya, K. Hayasaka, Y. Takeda, T. Fukuda, D. Kumaki and S. Tokito, A Printed Organic Circuit System for Wearable Amperometric Electrochemical Sensors, *Scientific Reports*, 2018, **8**, 6368.

98 Y.-F. Wang, T. Sekine, Y. Takeda, K. Yokosawa, H. Matsui, D. Kumaki, T. Shiba, T. Nishikawa and S. Tokito, Fully Printed PEDOT:PSS-based Temperature Sensor with High Humidity Stability for Wireless Healthcare Monitoring, *Sci Rep*, 2020, **10**, 2467.

99 P. Lorwongtragool, E. Sowade, N. Watthanawisuth, R. Baumann and T. Kerdcharoen, A Novel Wearable Electronic Nose for Healthcare Based on Flexible Printed Chemical Sensor Array, *Sensors*, 2014, **14**, 19700–19712.

100 Y. Jin, G. Chen, K. Lao, S. Li, Y. Lu, Y. Gan, Z. Li, J. Hu, J. Huang, J. Wen, H. Deng, M. Yang, Z. Chen, X. Hu, B. Liang and J. Luo, Identifying human body states by using a flexible integrated sensor, *npj Flex Electron*, 2020, **4**, 28.

101 I. Wicaksono, C. I. Tucker, T. Sun, C. A. Guerrero, C. Liu, W. M. Woo, E. J. Pence and C. Dagdeviren, A tailored, electronic textile conformable suit for large-scale spatiotemporal physiological sensing in vivo, *npj Flex Electron*, 2020, **4**, 1–13.

102 E. O. Polat, G. Mercier, I. Nikitskiy, E. Puma, T. Galan, S. Gupta, M. Montagut, J. J. Piqueras, M. Bouwens, T. Durduran, G. Konstantatos, S. Goossens and F. Koppens, Flexible graphene photodetectors for wearable fitness monitoring, *Science Advances*, 2019, **5**, eaaw7846.

103 A. Shamim, in *2017 International Symposium on Antennas and Propagation (ISAP)*, IEEE, Phuket, 2017, pp. 1–2.

104 S.-J. Woo, J.-H. Kong, D.-G. Kim and J.-M. Kim, A thin all-elastomeric capacitive pressure sensor array based on micro-contact printed elastic conductors, *J. Mater. Chem. C*, 2014, **2**, 4415–4422.

105 D.-L. Wen, X. Liu, H.-T. Deng, D.-H. Sun, H.-Y. Qian, J. Brugger and X.-S. Zhang, Printed silk-fibroin-based triboelectric nanogenerators for multi-functional wearable sensing, *Nano Energy*, 2019, **66**, 104123.

106 P. Maharjan, H. Cho, M. S. Rasel, Md. Salauddin and J. Y. Park, A fully enclosed, 3D printed, hybridized nanogenerator with flexible flux concentrator for harvesting diverse human biomechanical energy, *Nano Energy*, 2018, **53**, 213–224.

107 A. M. Gaikwad, J. W. Gallaway, D. Desai and D. A. Steingart, Electrochemical-Mechanical Analysis of Printed Silver Electrodes in a Microfluidic Device, *J. Electrochem. Soc.*, 2010, **158**, A154.

108 A. Al-Halhouli, L. Al-Ghussain, O. Khallouf, A. Rabadi, J. Alawadi, H. Liu, K. Al Oweidat, F. Chen and D. Zheng, Clinical Evaluation of Respiratory Rate Measurements on COPD (Male) Patients Using Wearable Inkjet-Printed Sensor, *Sensors*, 2021, **21**, 468.

109 A. Al-Halhouli, L. Al-Ghussain, S. El Bouri, H. Liu and D. Zheng, Fabrication and Evaluation of a Novel Non-Invasive Stretchable and Wearable Respiratory Rate Sensor Based on Silver Nanoparticles Using Inkjet Printing Technology, *Polymers*, 2019, **11**, 1518.

110 L.-W. Lo, H. Shi, H. Wan, Z. Xu, X. Tan and C. Wang, Inkjet-Printed Soft Resistive Pressure Sensor Patch for Wearable Electronics Applications, *Advanced Materials Technologies*, 2020, **5**, 1900717.

111 J. Abu-Khalaf, R. Saraireh, S. Eisa and A. Al-Halhouli, Experimental Characterization of Inkjet-Printed Stretchable Circuits for Wearable Sensor Applications, *Sensors*, 2018, **18**, 3476.

112 R. Sliz, Reliability of R2R-printed, flexible electrodes for e-clothing applications, *npj Flexible Electronics*, 2020, 9.

113 S. Ali, S. Khan and A. Bermak, Inkjet-Printed Human Body Temperature Sensor for Wearable Electronics, *IEEE Access*, 2019, **7**, 163981–163987.

114 H. Kao, C.-H. Chuang, L.-C. Chang, C.-L. Cho and H.-C. Chiu, Inkjet-printed silver films on textiles for wearable electronics applications, *Surface and Coatings Technology*, 2019, **362**, 328–332.

115 M. F. Farooqui and A. Shamim, Low Cost Inkjet Printed Smart Bandage for Wireless Monitoring of Chronic Wounds, *Sci Rep*, 2016, **6**, 28949.

116 V.-T. Tran, Y. Wei, H. Yang, Z. Zhan and H. Du, All-inkjet-printed flexible ZnO micro photodetector for a wearable UV monitoring device, *Nanotechnology*, 2017, **28**, 095204.

117 D. J. Finn, M. Lotya and J. N. Coleman, Inkjet Printing of Silver Nanowire Networks, *ACS Appl. Mater. Interfaces*, 2015, **7**, 9254–9261.

118 J. D. Park, S. Lim and H. Kim, Patterned silver nanowires using the gravure printing process for flexible applications, *Thin Solid Films*, 2015, **586**, 70–75.

119 Q. Huang and Y. Zhu, Patterning of Metal Nanowire Networks: Methods and Applications, *ACS Appl. Mater. Interfaces*, 2021, **13**, 60736–60762.

120 A. M. Zamarayeva, A. E. Ostfeld, M. Wang, J. K. Duey, I. Deckman, B. P. Lechêne, G. Davies, D. A. Steingart and A. C. Arias, Flexible and stretchable power sources for wearable electronics, *Science Advances*, 2017, **3**, e1602051.

121 D. Khodagholy, J. N. Gelinas, Z. Zhao, M. Yeh, M. Long, J. D. Greenlee, W. Doyle, O. Devinsky and G. Buzsáki, Organic electronics for high-resolution electrocorticography of the human brain, *Science Advances*, 2016, **2**, e1601027.

122 Y. Khan, M. Garg, Q. Gui, M. Schadt, A. Gaikwad, D. Han, N. A. D. Yamamoto, P. Hart, R. Welte, W. Wilson, S. Czarnecki, M. Poliks, Z. Jin, K. Ghose, F. Egitto, J. Turner and A. C. Arias, Flexible Hybrid Electronics: Direct Interfacing of Soft and Hard Electronics for Wearable Health Monitoring, *Adv. Funct. Mater.*, 2016, **26**, 8764–8775.

123 N. Karim, S. Afroj, A. Malandraki, S. Butterworth, C. Beach, M. Rigout, K. S. Novoselov, A. J. Casson and S. G. Yeates, All inkjet-printed graphene-based conductive patterns for wearable e-textile applications, *J. Mater. Chem. C*, 2017, **5**, 11640–11648.

124 B. Krykpayev, M. F. Farooqui, R. M. Bilal, M. Vaseem and A. Shamim, A wearable tracking device inkjet-printed on textile, *Microelectronics Journal*, 2017, **65**, 40–48.

125 A. Sajedi-Moghaddam, E. Rahmanian and N. Naseri, Inkjet-Printing Technology for Supercapacitor Application: Current State and Perspectives, *ACS Appl. Mater. Interfaces*, 2020, **12**, 34487–34504.

126 B.-J. de Gans, P. C. Duineveld and U. S. Schubert, Inkjet Printing of Polymers: State of the Art and Future Developments, *Advanced Materials*, 2004, **16**, 203–213.

127 Y.-Z. Zhang, Y. Wang, T. Cheng, W.-Y. Lai, H. Pang and W. Huang, Flexible supercapacitors based on paper substrates: a new paradigm for low-cost energy storage, *Chem. Soc. Rev.*, 2015, **44**, 5181–5199.

128 H. Sirringhaus, T. Kawase, R. H. Friend, T. Shimoda, M. Inbasekaran, W. Wu and E. P. Woo, High-resolution inkjet printing of all-polymer transistor circuits, *Science*, 2000, **290**, 2123–2126.

129 Y.-Z. Zhang, Y. Wang, T. Cheng, L.-Q. Yao, X. Li, W.-Y. Lai and W. Huang, Printed supercapacitors: materials, printing and applications, *Chem. Soc. Rev.*, 2019, **48**, 3229–3264.

130 B. Derby, Inkjet Printing of Functional and Structural Materials: Fluid Property Requirements, Feature Stability, and Resolution, *Annu. Rev. Mater. Res.*, 2010, **40**, 395–414.

131 P. C. Duineveld, M. M. de Kok, M. Buechel, A. Sempel, K. A. H. Mutsaers, P. van de Weijer, I. G. J. Camps, T. van de Biggelaar, J.-E. J. M. Rubingh and E. I. Haskal, ed. Z. H. Kafafi, San Diego, CA, USA, 2002, p. 59.

132 C. D. Stow, M. G. Hadfield and J. M. Ziman, An experimental investigation of fluid flow resulting from the impact of a water drop with an unyielding dry surface, *Proceedings of the Royal Society of London. A. Mathematical and Physical Sciences*, 1981, **373**, 419–441.

133 R. Bhola and S. Chandra, Parameters controlling solidification of molten wax droplets falling on a solid surface, *Journal of Materials Science*, 1999, **34**, 4883–4894.

134 J. Li, F. Rossignol and J. Macdonald, Inkjet printing for biosensor fabrication: combining chemistry and technology for advanced manufacturing, *Lab Chip*, 2015, **15**, 2538–2558.

135 N. Mohan, S. K. Bhogaraju, M. Lysien, L. Schneider, F. Granek, K. Lux and G. Elger, in *2021 23rd European Microelectronics and Packaging Conference & Exhibition (EMPC)*, IEEE, Gothenburg, Sweden, 2021, pp. 1–6.

136 G. D. Martin, S. D. Hoath and I. M. Hutchings, Inkjet printing - the physics of manipulating liquid jets and drops, *J. Phys.: Conf. Ser.*, 2008, **105**, 012001.

137 B. Derby, Inkjet Printing of Functional and Structural Materials: Fluid Property Requirements, Feature Stability, and Resolution, *Annu. Rev. Mater. Res.*, 2010, **40**, 395–414.

138 J. Wang, B. Yiu, J. Obermeyer, C. D. M. Filipe, J. D. Brennan and R. Pelton, Effects of Temperature and Relative Humidity on the Stability of Paper-Immobilized Antibodies, *Biomacromolecules*, 2012, **13**, 559–564.

139 A. L. Yarin, DROP IMPACT DYNAMICS: Splashing, Spreading, Receding, Bouncing…, *Annual Review of Fluid Mechanics*, 2006, **38**, 159–192.

140 R. Rioboo, M. Marengo and C. Tropea, Time evolution of liquid drop impact onto solid, dry surfaces, *Experiments in Fluids*, 2002, **33**, 112–124.

141 K. Yan, J. Li, L. Pan and Y. Shi, Inkjet printing for flexible and wearable electronics, *APL Materials*, 2020, **8**, 120705.

142 P. C. Duineveld, The stability of ink-jet printed lines of liquid with zero receding contact angle on a homogeneous substrate, *Journal of Fluid Mechanics*, 2003, **477**, 175–200.

143 M. Gao, L. Li and Y. Song, Inkjet printing wearable electronic devices, *J. Mater. Chem. C*, 2017, **5**, 2971–2993.

144 X. Yang, V. H. Chhasatia, J. Shah and Y. Sun, Coalescence, evaporation and particle deposition of consecutively printed colloidal drops, *Soft Matter*, 2012, **8**, 9205.

145 D. Soltman and V. Subramanian, Inkjet-printed line morphologies and temperature control of the coffee ring effect, *Langmuir*, 2008, **24**, 2224–2231.

146 R. D. Deegan, O. Bakajin, T. F. Dupont, G. Huber, S. R. Nagel and T. A. Witten, Capillary flow as the cause of ring stains from dried liquid drops, *Nature*, 1997, **389**, 827–829.

147 R. D. Deegan, O. Bakajin, T. F. Dupont, G. Huber, S. R. Nagel and T. A. Witten, Contact line deposits in an evaporating drop, *Phys. Rev. E*, 2000, **62**, 756–765.

148 R. D. Deegan, Pattern formation in drying drops, *Phys. Rev. E*, 2000, **61**, 475–485.

149 Y. Kim, X. Ren, J. W. Kim and H. Noh, Direct inkjet printing of micro-scale silver electrodes on polydimethylsiloxane (PDMS) microchip, *J. Micromech. Microeng.*, 2014, **24**, 115010.

150 P. J. Smith, D.-Y. Shin, J. E. Stringer, B. Derby and N. Reis, Direct ink-jet printing and low temperature conversion of conductive silver patterns, *J Mater Sci*, 2006, **41**, 4153–4158.

151 X. Yu, R. Xing, Z. Peng, Y. Lin, Z. Du, J. Ding, L. Wang and Y. Han, To inhibit coffee ring effect in inkjet printing of light-emitting polymer films by decreasing capillary force, *Chinese Chemical Letters*, 2019, **30**, 135–138.

152 Y. Li, Q. Yang, M. Li and Y. Song, Rate-dependent interface capture beyond the coffee-ring effect, *Sci Rep*, 2016, **6**, 24628.

153 W. D. Ristenpart, P. G. Kim, C. Domingues, J. Wan and H. A. Stone, Influence of Substrate Conductivity on Circulation Reversal in Evaporating Drops, *Phys. Rev. Lett.*, 2007, **99**, 234502.

154 G. Hu, T. Albrow-Owen, X. Jin, A. Ali, Y. Hu, R. C. T. Howe, K. Shehzad, Z. Yang, X. Zhu, R. I. Woodward, T.-C. Wu, H. Jussila, J.-B. Wu, P. Peng, P.-H. Tan, Z. Sun, E. J. R. Kelleher, M. Zhang, Y. Xu and T. Hasan, Black phosphorus ink formulation for inkjet printing of optoelectronics and photonics, *Nat Commun*, 2017, **8**, 278.

155 Y. Liu, F. Li, L. Qiu, K. Yang, Q. Li, X. Zheng, H. Hu, T. Guo, C. Wu and T. W. Kim, Fluorescent Microarrays of in Situ Crystallized Perovskite Nanocomposites Fabricated for Patterned Applications by Using Inkjet Printing, *ACS Nano*, 2019, **13**, 2042–2049.

156 K. N. Al-Milaji, R. R. Secondo, T. N. Ng, N. Kinsey and H. Zhao, Interfacial Self-Assembly of Colloidal Nanoparticles in Dual-Droplet Inkjet Printing, *Adv. Mater. Interfaces*, 2018, **5**, 1701561.

157 E. He, D. Guo and Z. Li, A Widely Applicable Strategy for Coffee-Ring Effect Suppression and Controllable Deposition of Nanoparticles Utilizing Ice Drying, *Advanced Materials Interfaces*, 2019, **6**, 1900446.

158 J. Ding, J. Liu, Q. Tian, Z. Wu, W. Yao, Z. Dai, L. Liu and W. Wu, Preparing of Highly Conductive Patterns on Flexible Substrates by Screen Printing of Silver Nanoparticles with Different Size Distribution, *Nanoscale Res Lett*, 2016, **11**, 412.

159 Dimatix Materials Printer DMP-2850 | Fujifilm [United States], https://www.fujifilm.com/us/en/business/inkjet-solutions/inkjet-technology-integration/dmp-2850, (accessed 26 February 2022).

160 A. Al-Halhouli, H. Qitouqa, A. Alashqar and J. Abu-Khalaf, Inkjet printing for the fabrication of flexible/stretchable wearable electronic devices and sensors, *Sensor Review*, 2018, **38**, 438–452.

161 N. Ibrahim, J. O. Akindoyo and M. Mariatti, Recent development in silver-based ink for flexible electronics, *Journal of Science: Advanced Materials and Devices*, 2022, **7**, 100395.

162 H.-M. Ren, Y. Guo, S.-Y. Huang, K. Zhang, M. M. F. Yuen, X.-Z. Fu, S. Yu, R. Sun and C.-P. Wong, One-Step Preparation of Silver Hexagonal Microsheets as Electrically Conductive

Adhesive Fillers for Printed Electronics, *ACS Appl. Mater. Interfaces*, 2015, **7**, 13685–13692.

163 I. J. Fernandes, A. F. Aroche, A. Schuck, P. Lamberty, C. R. Peter, W. Hasenkamp and T. L. A. C. Rocha, Silver nanoparticle conductive inks: synthesis, characterization, and fabrication of inkjet-printed flexible electrodes, *Sci Rep*, 2020, **10**, 8878.

164 N. Karim, S. Afroj, A. Malandraki, S. Butterworth, C. Beach, M. Rigout, K. S. Novoselov, A. J. Casson and S. G. Yeates, All inkjet-printed graphene-based conductive patterns for wearable e-textile applications, *J. Mater. Chem. C*, 2017, **5**, 11640–11648.

165 J. Yang, K. Ling, L. Liu, X. Zeng, X. Xu, Z. Li and P. He, Printable and Wearable Graphene-Based Strain Sensor With High Sensitivity for Human Motion Monitoring, *IEEE Sensors J.*, 2022, **22**, 13937–13944.

166 D. McManus, S. Vranic, F. Withers, V. Sanchez-Romaguera, M. Macucci, H. Yang, R. Sorrentino, K. Parvez, S.-K. Son, G. Iannaccone, K. Kostarelos, G. Fiori and C. Casiraghi, Water-based and biocompatible 2D crystal inks for all-inkjet-printed heterostructures, *Nature Nanotech*, 2017, **12**, 343–350.

167 X. Liang, H. Li, J. Dou, Q. Wang, W. He, C. Wang, D. Li, J. Lin and Y. Zhang, Stable and Biocompatible Carbon Nanotube Ink Mediated by Silk Protein for Printed Electronics, *Adv. Mater.*, 2020, **32**, 2000165.

168 A. A. Kazemzadeh Farizhandi, S. Z. Khalajabadi, V. Krishnadoss and I. Noshadi, Synthesized biocompatible and conductive ink for 3D printing of flexible electronics, *Journal of the Mechanical Behavior of Biomedical Materials*, 2020, **110**, 103960.

169 X. Li, M. Li, L. Zong, X. Wu, J. You, P. Du and C. Li, Liquid Metal Droplets Wrapped with Polysaccharide Microgel as Biocompatible Aqueous Ink for Flexible Conductive Devices, *Adv. Funct. Mater.*, 2018, **28**, 1804197.

170 F. Zhao, Y. Shi, L. Pan and G. Yu, Multifunctional Nanostructured Conductive Polymer Gels: Synthesis, Properties, and Applications, *Acc. Chem. Res.*, 2017, **50**, 1734–1743.

171 L. Pan, G. Yu, D. Zhai, H. R. Lee, W. Zhao, N. Liu, H. Wang, B. C.-K. Tee, Y. Shi, Y. Cui and Z. Bao, Hierarchical nanostructured conducting polymer hydrogel with high electrochemical activity, *Proceedings of the National Academy of Sciences*, 2012, **109**, 9287–9292.

172 L. Li, Y. Wang, L. Pan, Y. Shi, W. Cheng, Y. Shi and G. Yu, A Nanostructured Conductive Hydrogels-Based Biosensor Platform for Human Metabolite Detection, *Nano Lett.*, 2015, **15**, 1146–1151.

173 D. Zhai, B. Liu, Y. Shi, L. Pan, Y. Wang, W. Li, R. Zhang and G. Yu, Highly Sensitive Glucose Sensor Based on Pt Nanoparticle/Polyaniline Hydrogel Heterostructures, *ACS Nano*, 2013, **7**, 3540–3546.

174 Z. Ma, W. Shi, K. Yan, L. Pan and G. Yu, Doping engineering of conductive polymer hydrogels and their application in advanced sensor technologies, *Chem. Sci.*, 2019, **10**, 6232–6244.

175 J. Xu, H.-C. Wu, C. Zhu, A. Ehrlich, L. Shaw, M. Nikolka, S. Wang, F. Molina-Lopez, X. Gu, S. Luo, D. Zhou, Y.-H. Kim, G.-J. N. Wang, K. Gu, V. R. Feig, S. Chen, Y. Kim, T. Katsumata, Y.-Q. Zheng, H. Yan, J. W. Chung, J. Lopez, B. Murmann and Z. Bao, Multi-scale ordering in highly stretchable polymer semiconducting films, *Nat. Mater.*, 2019, **18**, 594–601.

176 S. G. Bucella, A. Luzio, E. Gann, L. Thomsen, C. R. McNeill, G. Pace, A. Perinot, Z. Chen, A. Facchetti and M. Caironi, Macroscopic and high-throughput printing of aligned nanostructured polymer semiconductors for MHz large-area electronics, *Nat Commun*, 2015, **6**, 8394.

177 A. Perinot and M. Caironi, Accessing MHz Operation at 2 V with Field-Effect Transistors Based on Printed Polymers on Plastic, *Advanced Science*, 2019, **6**, 1801566.

178 L. Bu, M. Hu, W. Lu, Z. Wang and G. Lu, Printing Semiconductor–Insulator Polymer Bilayers for High-Performance Coplanar Field-Effect Transistors, *Advanced Materials*, 2018, **30**, 1704695.

179 ramé-hart instrument co. Monthly Newsletter, http://www.ramehart.com/newsletters/2021-03_news.htm, (accessed 26 February 2022).

180 C.-Y. Li and Y.-C. Liao, Adhesive Stretchable Printed Conductive Thin Film Patterns on PDMS Surface with an Atmospheric Plasma Treatment, *ACS Appl. Mater. Interfaces*, 2016, **8**, 11868–11874.

181 C. de Menezes Atayde and I. Doi, Highly stable hydrophilic surfaces of PDMS thin layer obtained by UV radiation and oxygen plasma treatments, *Phys. Status Solidi (c)*, 2010, **7**, 189–192.

182 S. H. Tan, N.-T. Nguyen, Y. C. Chua and T. G. Kang, Oxygen plasma treatment for reducing hydrophobicity of a sealed polydimethylsiloxane microchannel, *Biomicrofluidics*, 2010, **4**, 032204.

183 J. Sun, J. Jiang, B. Bao, S. Wang, M. He, X. Zhang and Y. Song, Fabrication of Bendable Circuits on a Polydimethylsiloxane (PDMS) Surface by Inkjet Printing Semi-Wrapped Structures, *Materials (Basel)*, 2016, **9**, 253.

184 J. Wu, R. C. Roberts, N. C. Tien and D. Li, in *IEEE SENSORS 2014 Proceedings*, IEEE, Valencia, Spain, 2014, pp. 1100–1103.

185 R. Mikkonen and M. Mantysalo, in *2020 IEEE International Conference on Flexible and Printable Sensors and Systems (FLEPS)*, IEEE, Manchester, United Kingdom, 2020, pp. 1–3.

186 K. N. Al-Milaji, Q. Huang, Z. Li, T. N. Ng and H. Zhao, Direct Embedment and Alignment of Silver Nanowires by Inkjet Printing for Stretchable Conductors, *ACS Appl. Electron. Mater.*, 2020, **2**, 3289–3298.

187 J. M. Abu-Khalaf, L. Al-Ghussain and A. Al-Halhouli, Fabrication of Stretchable Circuits on Polydimethylsiloxane (PDMS) Pre-Stretched Substrates by Inkjet Printing Silver Nanoparticles, *Materials (Basel)*, 2018, **11**, 2377.

188 J. Lee, S. Chung, H. Song, S. Kim and Y. Hong, Lateral-crack-free, buckled, inkjet-printed silver electrodes on highly pre-stretched elastomeric substrates, *J. Phys. D: Appl. Phys.*, 2013, **46**, 105305.

189 D. Qi, K. Zhang, G. Tian, B. Jiang and Y. Huang, Stretchable Electronics Based on PDMS Substrates, *Advanced Materials*, 2021, **33**, 2003155.

190 S. Chung, J. Lee, H. Song, S. Kim, J. Jeong and Y. Hong, Inkjet-printed stretchable silver electrode on wave structured elastomeric substrate, *Appl. Phys. Lett.*, 2011, **98**, 153110.

191 J. Jiang, B. Bao, M. Li, J. Sun, C. Zhang, Y. Li, F. Li, X. Yao and Y. Song, Fabrication of Transparent Multilayer Circuits by Inkjet Printing, *Advanced Materials*, 2016, **28**, 1420–1426.

192 A. Larmagnac, S. Eggenberger, H. Janossy and J. Vörös, Stretchable electronics based on Ag-PDMS composites, *Sci Rep*, 2014, **4**, 7254.

193 A. Claypole, J. Claypole, L. Kilduff, D. Gethin and T. Claypole, Stretchable Carbon and Silver Inks for Wearable Applications, *Nanomaterials*, 2021, **11**, 1200.

194 J. F. Christ, N. Aliheidari, P. Pötschke and A. Ameli, Bidirectional and Stretchable Piezoresistive Sensors Enabled by Multimaterial 3D Printing of Carbon Nanotube/Thermoplastic Polyurethane Nanocomposites, *Polymers*, 2019, **11**, 11.

195 D. Gao, J. Wang, K. Ai, J. Xiong, S. Li and P. S. Lee, Inkjet-Printed Iontronics for Transparent, Elastic, and Strain-Insensitive Touch Sensing Matrix, *Advanced Intelligent Systems*, 2020, **2**, 2000088.

196 UMass patch would spot stressed-out soldiers - The Boston Globe, https://www.bostonglobe.com/business/2014/08/03/umass-scientists-working-patch-that-measures-stress/X7MEkIZDz3Mwalb1NY3PNL/story.html, (accessed 15 June 2021).

197 D. P. Rose, M. E. Ratterman, D. K. Griffin, L. Hou, N. Kelley-Loughnane, R. R. Naik, J. A. Hagen, I. Papautsky and J. C. Heikenfeld, Adhesive RFID Sensor Patch for Monitoring of Sweat Electrolytes, *IEEE Trans. Biomed. Eng.*, 2015, **62**, 1457–1465.

198 J. Chen, Y. Zhou, D. Wang, F. He, V. M. Rotello, K. R. Carter, J. J. Watkins and S. R. Nugen, UV-nanoimprint lithography as a tool to develop flexible microfluidic devices for electrochemical detection, *Lab Chip*, 2015, **15**, 3086–3094.

199 F. He and S. R. Nugen, Automating fluid delivery in a capillary microfluidic device using low-voltage electrowetting valves, *Microfluid Nanofluid*, 2014, **16**, 879–886.

200 S. R. Nugen, P. J. Asiello, J. T. Connelly and A. J. Baeumner, PMMA biosensor for nucleic acids with integrated mixer and electrochemical detection, *Biosensors and Bioelectronics*, 2009, **24**, 2428–2433.

201 J. Morse, Y. Zhao, V. Rotello, S. Nugen and J. Watkins, in *2016 6th Electronic System-Integration Technology Conference (ESTC)*, IEEE, Grenoble, France, 2016, pp. 1–3.

202 U.S. Environmental Protection Agency | US EPA, https://www.epa.gov/, (accessed 26 February 2022).